THE GEOLOGICAL SOCIETY OF AMERICA®

Temporal and spatial variations in magmatism and transpression in a Cretaceous arc, Median Batholith, Fiordland, New Zealand

Luisa F. Buriticá[1], Joshua J. Schwartz[1,*], Keith A. Klepeis[2], Elena A. Miranda[1], Andy J. Tulloch[3], Matthew A. Coble[4], and Andrew R.C. Kylander-Clark[5]

[1]DEPARTMENT OF GEOLOGY, CALIFORNIA STATE UNIVERSITY, NORTHRIDGE, CALIFORNIA 91330, USA
[2]DEPARTMENT OF GEOLOGY, THE UNIVERSITY OF VERMONT, BURLINGTON, VERMONT 05405, USA
[3]GNS SCIENCE, PRIVATE BAG 1930, DUNEDIN, NEW ZEALAND
[4]SCHOOL OF EARTH, ENERGY AND ENVIRONMENTAL SCIENCES, STANFORD UNIVERSITY, STANFORD, CALIFORNIA 94305, USA
[5]DEPARTMENT OF EARTH SCIENCE, UNIVERSITY OF CALIFORNIA–SANTA BARBARA, SANTA BARBARA, CALIFORNIA 93106, USA

ABSTRACT

We investigated the interplay between deformation and pluton emplacement with the goal of providing insights into the role of transpression and arc magmatism in forming and modifying continental arc crust. We present 39 new laser-ablation–split-stream–inductively coupled plasma–mass spectrometry (LASS-ICP-MS) and secondary ion mass spectrometry (SIMS) $^{206}Pb/^{238}U$ zircon and titanite dates, together with titanite geochemistry and temperatures from the lower and middle crust of the Mesozoic Median Batholith, New Zealand, to (1) constrain the timing of Cretaceous arc magmatism in the Separation Point Suite, (2) document the timing of titanite growth in low- and high-strain deformational fabrics, and (3) link spatial and temporal patterns of lithospheric-scale transpressional shear zone development to the Cretaceous arc flare-up event. Our zircon results reveal that Separation Point Suite plutonism lasted from ca. 129 Ma to ca. 110 Ma in the middle crust of eastern and central Fiordland. Deformation during this time was focused into a 20-km-wide, arc-parallel zone of deformation that includes previously unreported segments of a complex shear zone that we term the Grebe shear zone. Early deformation in the Grebe shear zone involved development of low-strain fabrics with shallowly plunging mineral stretching lineations from ca. 129 to 125 Ma. Titanites in these rocks are euhedral, are generally aligned with weak subsolidus fabrics, and give rock-average temperatures ranging from 675 °C to 700 °C. We interpret them as relict magmatic titanites that grew prior to low-strain fabric development. In contrast, deformation from ca. 125 to 116 Ma involved movement along subvertical, mylonitic shear zones with moderately to steeply plunging mineral stretching lineations. Titanites in these shear zones are anhedral grains/aggregates that are aligned within mylonitic fabrics and have rock-average temperatures ranging from ~610 °C to 700 °C. These titanites are most consistent with (re)crystallization in response to deformation and/or metamorphic reactions during amphibolite-facies metamorphism. At the orogen scale, spatial and temporal patterns indicate that the Separation Point Suite flare-up commenced during low-strain deformation in the middle crust (ca. 129–125 Ma) and peaked during high-strain, transpressional deformation (ca. 125–116 Ma), during which time the magmatic arc axis widened to 70 km or more. We suggest that transpressional deformation during the arc flare-up event was an important process in linking melt storage regions and controlling the distribution and geometry of plutons at mid-crustal levels.

LITHOSPHERE GSA Data Repository Item 2019309 https://doi.org/10.1130/L1073.1

INTRODUCTION

Cordilleran arcs are locations of continental crust formation and stabilization (Ducea et al., 2015; Cawood et al., 2013; Kelemen et al., 2013; Jagoutz and Kelemen, 2015). An outstanding question in petrology and continental tectonics is how the architecture of the arc is affected by the interaction between deformation and magmatic processes (Brown and Solar, 1998; Matzel et al., 2006; Weinberg et al., 2009; Sen et al., 2014). The apparent spatial correlation between regional structures and plutons has fueled debate on the way(s) in which magmatic emplacement processes are influenced by the stress field within the arc. Additionally, there is uncertainty regarding whether magmatism and deformation are coupled, and the time scales over which coupling may occur (Vigneresse, 1995; Blanquat et al., 1998; Paterson and Schmidt, 1999; Schmidt and Paterson, 2000; Vigneresse and Clemens, 2000). Thus, reconstructions of the emplacement and deformation history of batholiths are important to our understanding of magmatic arc construction and continental crust growth.

Most modern continental arcs occur in oblique convergent settings, where transpressional and contractional regimes are common (Harland, 1971; Fossen et al., 1994; Blanquat et al., 1998). Transpression refers to strike-slip deformation that simultaneously accommodates horizontal shortening and vertical extrusion (Harland, 1971; Sanderson and Marchini, 1984; Fossen et al., 1994; Dewey et al., 1998). Harland (1971) and Blanquat et al. (1998) described transpression as the dominant deformation process

*Corresponding author: joshua.schwartz@csun.edu

in oblique convergent systems, where strain is accommodated within the magmatic arc, due mainly to the development of three-dimensional noncoaxial strain, high heat flow, and rheological contrasts. Continental arcs are therefore ideal places to study the interaction between transpressional deformation and generation/transport of arc magmas.

Transpressional deformation during magmatism has been proposed to be important for the mobilization of magma through the continental crust (Weinberg et al., 2004; Marcotte et al., 2005; Whitney et al., 2009; Pereira et al., 2013). Other workers, however, have suggested that changes in the thermal gradient of country rocks dominantly control magma transport (Vigneresse, 1995; Johnson, 2009). The interplay between pluton emplacement and transpression at different crustal levels is still poorly understood; consequently, an enhanced understanding of the way(s) in which magma is transferred and emplaced within continental arcs during periods of regional deformation can elucidate a fundamental question in the evolution of continental crust and magmatic arc systems (e.g., Paterson et al., 1998; Paterson and Schmidt, 1999; Blanquat et al., 1998; Vigneresse and Clemens, 2000; Pereira et al., 2013; Bitencourt and Nardi, 2000; Sen et al., 2014; Webber et al., 2015; Stuart et al., 2018).

Here, we explored the timing and duration of plutonism and deformational events across the lower and middle crust using the Cretaceous Median Batholith in Fiordland, New Zealand, as a case study. We documented the temporal and spatial variations in the development of shear zone fabrics and their relationships to pluton emplacement. High- and low-strain zones form parts of a lithospheric-scale network of shear zones formed within the context of a Cretaceous arc flare-up event in the Mesozoic Median Batholith (Klepeis et al., 2004; Marcotte et al., 2005; Allibone and Tulloch, 2008; Scott et al., 2009; Klepeis et al., 2016; Milan et al., 2017; Schwartz et al., 2017). The arc flare-up event was characterized by a voluminous surge of mafic to intermediate magmas in the lower and middle crust and formed in response to changes in lower-plate dynamics, perhaps related to a slab tear event (e.g., Decker et al., 2017). Fiordland is an ideal location in which to explore the temporal and spatial relationships between strain and magmatism because it preserves a history of prolonged (>150 m.y.) Mesozoic convergence along the southeast margin of Gondwana, which coincided in part with the development of regional contractional and transpressional structures (Mortimer et al., 1999b; Klepeis et al., 2003, 2004; Allibone and Tulloch, 2008; Allibone et al., 2009b). Fiordland also offers excellent exposures of a nearly complete, faulted and tilted magmatic arc section from 5 to 65 km depth (Klepeis et al., 2003, 2004, 2019; De Paoli et al., 2009; Daczko et al., 2009; Scott et al., 2009), which allows us to investigate temporal and spatial relationships as a function of depth in a continental arc setting. In Fiordland, middle-crustal rocks are well exposed in eastern and central Fiordland (15–35 km), and lower-crustal rocks are represented in western Fiordland (35–65 km; Klepeis et al., 2019, and references therein).

A key feature of both middle- and lower-crustal ductile shear zones in Fiordland is that they contain titanite, which is increasingly recognized as a powerful tool with which to fingerprint the timing, temperature, and petrogenesis of igneous and metamorphic systems (Frost et al., 2001; Kohn and Corrie, 2011; Kylander-Clark et al., 2013; Spencer et al., 2013; Stearns et al., 2015; Scibiorski et al., 2019). Titanite occurs in a wide variety of crustal rocks, including quartzofeldspathic igneous rocks, such as the Separation Point Suite (Scott et al., 2009; this study), and in amphibolite- to granulite-facies prograde and retrograde metamorphic rocks such as those that characterize various shear zones in the middle and lower crust of Fiordland (e.g., Schwartz et al., 2016). It is an ideal phase for examining the timing and conditions of shear zone development because it incorporates abundant U (Essex and Gromet, 2000; Frost et al., 2001; Flowers et al., 2005; Schwartz et al., 2016), it partitions Zr as a function of pressure and temperature, enabling its use as a thermobarometer (Hayden et al., 2008), and it can crystallize and/or recrystallize during changing pressure and temperature events associated with reactions with Ca- and Al-bearing phases such as calcite, clinopyroxene, plagioclase, epidote, and hornblende (Franz and Spear, 1985; Essex and Gromet, 2000; Frost et al., 2001).

Here, we present 39 new laser-ablation–split-stream–inductively coupled plasma–mass spectrometer (LASS-ICP-MS) and secondary ion microprobe mass spectrometer (SIMS) $^{206}Pb/^{238}U$ zircon and titanite dates, titanite geochemical data, and Zr-in-titanite temperatures, which allow us to (1) constrain the timing of a the Cretaceous arc flare-up event in the middle crust (i.e., the Separation Point Suite), (2) document the timing of titanite growth in low- and high-strain deformational fabrics, and (3) link spatial and temporal patterns of lithospheric-scale, transpressional shear zone development to the Cretaceous arc flare-up event. We find that Separation Point Suite plutonism in central Fiordland lasted from ca. 129 Ma to ca. 110 Ma and overlapped with transpressional deformation in both the middle (129–116 Ma) and lower crust (119–106 Ma) of the Median Batholith. In the middle crust, crystal-plastic deformation initiated in low-strain shear zones (129–125 Ma) shortly after emplacement of the Refrigerator Orthogneiss, one of the earliest phases of the Separation Point Suite. High-strain, mylonitic shear zones are documented in Lake Manapouri (and southward in Lake Hauroko: Scott et al., 2011), and in various diffuse shear zones in Lake Te Anau during the ca. 125–116 Ma interval. This latter phase of transpressional deformation was associated with a voluminous surge of high-Sr/Y magmatism and the widening of the magmatic arc to 70 km or more during the flare-up stage. During this event, melts were focused into a broad, 20-km-wide zone of transpressional deformation in the middle crust and were temporally and spatially associated with ductile deformation in lower-crustal shear zones at the same time. Transpressional deformation in the lower crust outlasted emplacement of the Western Fiordland Orthogneiss (125–120 Ma in northern Fiordland) by ~10–15 m.y., and transpression at all levels of the crust appears to have ceased prior to the initiation of extensional orogenic collapse in the lower crust at ca. 106 Ma.

GEOLOGIC SETTING AND PREVIOUS WORK

Zealandia and the Median Batholith

New Zealand is part of a submerged continental mass called Zealandia that broke apart from the supercontinent Gondwana in the Cretaceous (Luyendyk, 1995; Mortimer et al., 2017), and it records a history of Paleozoic to Mesozoic subduction-related plutonism and arc thickening and thinning, leading to extensional orogenic collapse in the Late Cretaceous (Mortimer, 2004). Zealandia can be divided into two provinces: the Western Province and Eastern Province (Irel and Gibson, 1998; Mortimer et al., 1999a; Meert, 2003; Klepeis and Clarke, 2004; Mortimer, 2004). The Western Province is composed of mid-Paleozoic subduction-related, S-type plutons as well as Paleozoic–Mesozoic volcanic and sedimentary rocks (Tulloch et al., 2009; Turnbull et al., 2016). The Eastern Province includes late Paleozoic–Mesozoic allochthonous terranes (Mortimer, 2004). The boundary between these two provinces is defined by the Median Batholith (Mortimer et al., 1999b; Scott, 2013), which has been offset ~480 km by Cenozoic dextral motion along the Alpine fault (e.g., Little et al., 2005).

Magmatic rocks in Zealandia range in age from Ordovician to Early Cretaceous (Fig. 1; Muir et al., 1998; Mortimer et al., 1999a; Tulloch and Kimbrough, 2003; Scott, 2013; Schwartz et al., 2017). Extensive Devonian to Carboniferous plutonic rocks occur throughout Fiordland and include the Karamea (S-type), Paringa (I-type), Foulwind (A-type), Ridge (S-type), and Tobin (I-type) suites (Tulloch et al., 2009; Turnbull et al., 2016). In

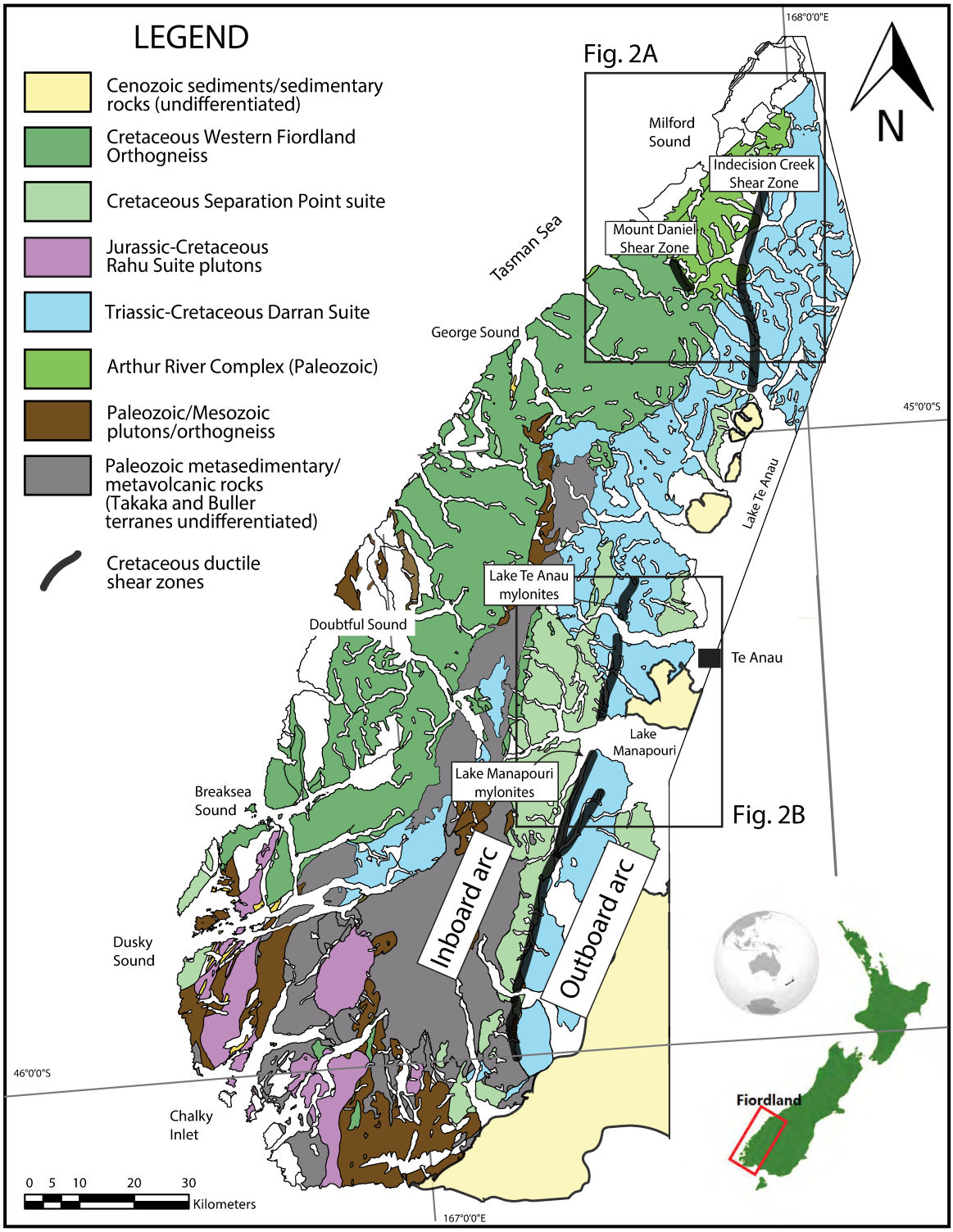

Figure 1. Geological map of the Fiordland sector of the Median Batholith, New Zealand. Study areas in northern Fiordland (Fig. 2A) and central Fiordland (Fig. 2B) are indicated by black squares (modified after Turnbull et al., 2010).

northern Fiordland, the Milford Gneiss (part of the Arthur River Complex) contains intensely metamorphosed and partially melted Late Devonian gneisses, which were subsequently intruded by Mesozoic plutonic rocks (Tulloch et al., 2011). Mesozoic plutonic rocks are subdivided into two belts (outboard and inboard), which are separated by the Grebe mylonite zone and its northern continuation, the Indecision Creek shear zone (Marcotte et al., 2005; Allibone et al., 2009a; Scott et al., 2011; Scott, 2013). These plutonic belts are composed of four different magmatic suites: (1) the inboard Western Fiordland Orthogneiss, which represents the deepest exposed portions of the arc (129–115 Ma; 35–65 km; Allibone et al., 2009b; De Paoli et al., 2009; Schwartz et al., 2016, 2017; Bhattacharya et al., 2018); (2) the inboard and outboard Separation Point Suite, composed of midcrustal calc-alkaline tonalites and granodiorites with high Sr/Y (>40) ratios (129–110 Ma; 15–35 km; Scott and Palin, 2008; Allibone et al., 2009a; Scott et al., 2009; this study); (3) the inboard Rahu Suite, consisting of upper- to midcrustal, Early Cretaceous I- and S-type granites (135–115 Ma; Golan et al., 2005; Allibone et al., 2009b; Ramezani and Tulloch, 2009); and (4) the inboard and outboard Darran Suite, with low-Sr/Y, Triassic to Early Cretaceous calc-alkaline plutons (235–136 Ma; 15–35 km; Kimbrough et al., 1994; Muir et al., 1998; Allibone et al., 2009a). In this study, we focused on magmatism associated with the inboard and outboard Separation Point Suite in central Fiordland (Figs. 1–2).

Several major intrabatholithic, transpressional shear zones were active before, during, and immediately after Cretaceous plutonism. In Fiordland and Stewart Island, these include, from north to south, the Anita shear zone (Klepeis et al., 1999; Czertowicz et al., 2016), Indecision Creek shear zone (Klepeis et al., 2004; Marcotte et al., 2005), the Mount Daniel shear zone (Klepeis et al., 2004), the George Sound shear zone (Klepeis et al., 2004), the Grebe mylonite zone (Figs. 2A–2B; Scott et al., 2011), and the Gutter shear zone (Stewart Island; Allibone and Tulloch, 2008). Scott et al. (2011) interpreted the Grebe mylonite zone as the boundary between the inboard and outboard belt in central Fiordland (Scott et al., 2011), and Marcotte et al. (2005) suggested that the Indecision Creek shear zone was the northern boundary between the inboard and outboard belts (Figs. 1 and 2). Both shear zones are described as transpressional in nature (Marcotte et al., 2005; Allibone and Tulloch, 2008; Scott et al., 2011; Klepeis et al., 2016), with the Indecision Creek shear zone and Grebe mylonite zone exposing lower and middle crust, respectively. Here, we focused on resolving temporal and spatial relationships between voluminous Early Cretaceous metamorphism and the development of these shear zones in central (middle crust) and northern Fiordland (lower crust).

METHODS

Sampling

Samples were collected from Lake Manapouri and Lake Te Anau in central Fiordland in January 2017 (Fig. 2B). Samples collected for

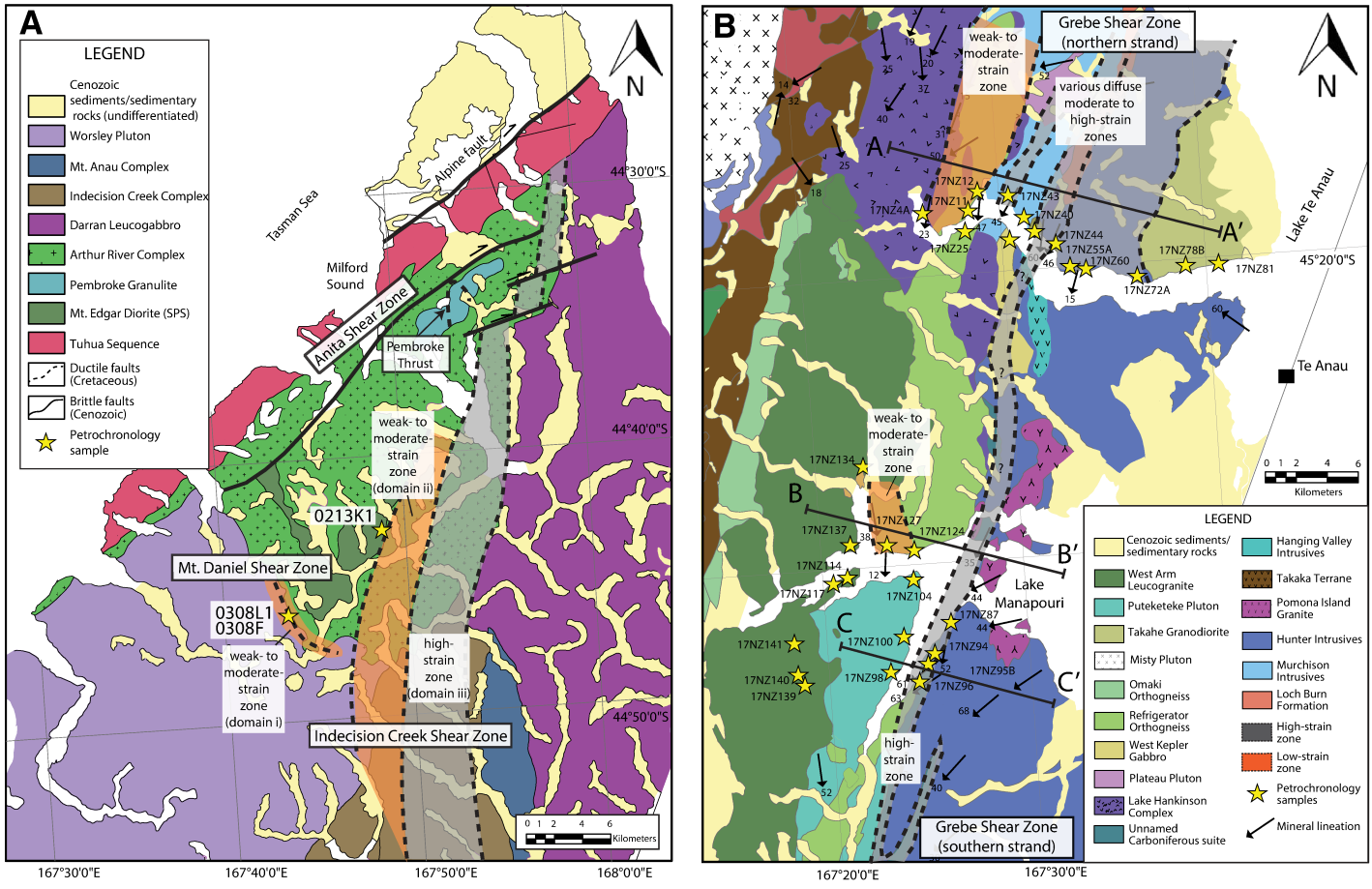

Figure 2. (A) Detailed geologic map of northern Fiordland and major structural features. (B) Detailed geologic map of central Fiordland and major structural features (modified after Turnbull et al., 2010). SPS—Separation Point Suite.

zircon geochronology included Separation Point Suite and Darran Suite plutonic rocks. Sample collection for titanite petrochronology focused on: (1) weakly to moderately foliated magmatic rocks in the Puteketeke Pluton in central Fiordland, (2) weakly deformed meta-igneous rocks in the Refrigerator Orthogneiss in central Fiordland, (3) strongly deformed and metamorphosed rocks in central Fiordland, and (4) weakly to moderately deformed rocks from the Mount Daniel shear zone (Klepeis et al., 2004) and the Indecision Creek shear zone in northern Fiordland (see locations in Figs. 2A–2B; Marcotte et al., 2005). Twenty-two zircon samples were analyzed by SIMS using the sensitive high-resolution mass spectrometer–reverse geometry (SHRIMP-RG) at Stanford University, cooperated by the U.S. Geological Survey, and 17 titanite-bearing samples were analyzed by LASS-ICP-MS at the University of California–Santa Barbara (UCSB). Additional geochronologic data used throughout this study were compiled from Marcotte et al. (2005), Schwartz et al. (2016, 2017), and Gebauer (2016).

Zircon and Titanite Geochronology

Zircon and titanite were separated using the standard mineral separation techniques at California State University–Northridge. Zircon analyses were performed on grains mounted in epoxy, and titanite was analyzed in situ using thin sections and grain mounts. Samples were sorted, cut, and prepared in Dunedin, New Zealand, at the Geological and Nuclear Sciences (GNS Science) rock laboratory facility. Thin sections and grain mounts were polished and imaged to avoid inclusions, cracks, and imperfections during the analytical sessions. Zircons were imaged by cathodoluminescence using a GatanMiniCL detector on an FEI Quanta 600 variable-pressure-setting scanning electron microscope (SEM), and titanite grains were imaged with the backscattered electron (BSE) detector at California State University–Northridge.

Twenty-two samples in four different epoxy mounts were analyzed for zircon U-Pb isotopes, as well as trace elements (Ti, Fe, Y, 9 rare earth elements [REEs], Hf, U, Th), following methods described by Coble et al. (2018). Depending on the abundance from mineral separates, between 60 and 100 zircons were picked and mounted per sample. Rims and cores were targeted for analysis in order to determine the timing of magmatism and/or metamorphism for all samples. Zircon spots with high common Pb were excluded from data analysis and plots. In cases where one or two grains were older than the majority of the zircon population, the older ages were presumed to represent inheritance, and this interpretation is supported by the differences in Th and U concentrations between core and rim spots (e.g., 17NZ94). Spots with statistically younger ages and large uncertainties were also excluded because they likely represent Pb loss. Zircon concordia plots and ages were created using IsoplotR (Vermeesch, 2018). Ages are presented as error-weighted average ages calculated from the common Pb–corrected $^{207}Pb/^{206}Pb$ and $^{238}U/^{206}Pb$ data.

The $^{206}Pb/^{238}U$ isotopes for titanite were collected using the LASS-ICP-MS at UCSB following methods outlined in Kylander-Clark et al. (2013), Spencer et al. (2013), and Schwartz et al. (2016). Depending on abundance, between 30 and 50 titanite grains per sample were picked and analyzed. Titanite data presented in this study were corrected for common Pb using a regression on the Tera-Wasserburg Pb/U isochron, where the *y* intercept will yield the $^{207}Pb/^{206}Pb$ isotopic ratio of the common Pb for each individual sample (Storey et al., 2006). Titanite ages are presented as lower intercepts calculated from regression of $^{207}Pb/^{206}Pb$ and $^{238}U/^{206}Pb$ data by IsoplotR (Vermeesch, 2018). The quoted titanite dates in the text and tables were assigned 2% uncertainties based on reproducibility of standards during analyses.

In simple systems where titanite dates are controlled by Pb volume diffusion, experimental studies suggest a closure temperature for titanite of ~650 °C, depending on grain size and cooling rate (Cherniak and Watson, 2000). Recent empirical studies from high-grade metamorphic rocks are somewhat at odds with the interpretation of titanite dates as recording closure temperatures (Kohn and Corrie, 2011; Spencer et al., 2013; Stearns et al., 2015; Schwartz et al., 2016). These studies show that titanite can preserve U-Pb dates (and Zr-in-titanite temperatures) at metamorphic conditions above 750 °C. A key finding in these studies is that Pb mobility in titanite is often driven by changing metamorphic conditions (pressure, temperature, fluid activity) rather than thermally activated volume diffusion. Moreover, Kirkland et al. (2016) suggested age information coupled with chemical and textural data can provide insight into conditions of titanite formation. Here, we integrated textures, trace-element geochemistry, and age dating to evaluate the origin of titanite in central and northern Fiordland.

Titanite Geochemistry and Thermometry

Titanite trace elements were measured by quadrupole LA-ICP-MS simultaneously with U-Pb isotopes measured by multicollector (MC) LA-ICP-MS at UCSB. Trace-element data were reduced using Iolite, and concentrations were calculated relative to BHVO as a primary standard. Model Zr-in-titanite temperatures were calculated following the methods from Hayden et al. (2008). Temperature uncertainties resulted from analytical uncertainties in the Zr measurements in titanite, which ranged from 3% to 12% (2σ). The activity of TiO_2 was assumed to be 0.7, based on the scarce presence of rutile or ilmenite in analyzed samples, and the activity of SiO_2 was assumed to equal 1.0 due to the presence of quartz. Pressure (*P*) was estimated for samples from central Fiordland at 0.6 GPa, while temperatures for samples in northern Fiordland were calculated with a pressure of 1.0 GPa (Daczko et al., 2002b; Scott et al., 2009; Scott, 2013; Marcotte et al., 2005; Stowell et al., 2010; Schwartz et al., 2016; Klepeis et al., 2016; Gebauer, 2016). Given the uncertainties in measurements, pressure values, and activities, we conservatively applied an uncertainty of ±50 °C to all our temperature estimates.

RESULTS

Field and Petrographic Observations

Central Fiordland

Field observations in central Fiordland revealed (1) magmatic structures (S_0), (2) subsolidus deformation in low- and moderate-strain zones characterized by shallowly dipping foliations (S_1) and shallowly plunging lineations (L_1), and (3) subsolidus deformation in high-strain zones characterized by moderately to steeply dipping foliations (S_2) and lineations (L_2) with amphibolite-facies mineral assemblages. Strain intensity in low- and high-strain zones was defined based on grain-size reduction (porphyroclast to matrix ratio), fabric intensity, and absence/presence of grain-shape alignment. Structural domains described herein and in Table 1 are strain-intensity dependent. Figure 3 shows three cross sections through central Fiordland illustrating the locations of these low- and high-strain zones and their host rocks.

Magmatic fabrics (S_0). These were observed in the Puteketeke Pluton and consist of weak to moderate planar alignment of biotite, hornblende, tabular plagioclase laths, and minor titanite that define a magmatic foliation (Figs. 4A–4B). Magmatic foliations are significantly shallower in dip relative to the high-strain zones and commonly dip 20°–50°. Magmatic layering is sometimes folded into outcrop-scale S and Z folds, the latter of which are characterized by top-to-the-SW vergence with fold limbs striking from 041° to 045° and dipping from 32° to 68° SE. In thin section, we

TABLE 1. SUMMARY OF STRUCTURAL AND GEOLOGICAL FEATURES IN CENTRAL FIORDLAND, LAKE TE ANAU AND LAKE MANAPOURI AREAS

Events	Unit	Structures	Orientations
S_0	Puteketeke Pluton	Magmatic foliations in tonalite and granodiorite	Striking 019°–085°, dipping 28°–54° southeast
S_1	Refrigerator Orthogneiss; Lake Hankinson Complex	Coarse- to medium-grained, subsolidus deformation in tonalite. Weak foliation with hbl, bt. Slightly aligned ttn in the fabric.	Striking 097°–166°, dipping 46°–90° southwest
L_1		Mineral stretching lineations with aligned hbl, bt, ttn	Southward trend with shallow south plunging 12°–40°
S_2	High-strain mylonite zones (Lake Manapouri mylonites; Lake Te Anau mylonites)	Moderate to strong mylonitic foliations with hbl, bt, ttn, czo. Aligned ttn in the fabric.	North-striking 65°–86°, west dipping
L_2		Mineral stretching lineations with aligned hbl, bt, ttn, czo	Southern trend with moderate south plunging 45°–65°

Note: Mineral abbreviations are after Whitney and Evans (2010): bt—biotite; czo—clinozoisite; hbl—hornblende; ttn—titanite.

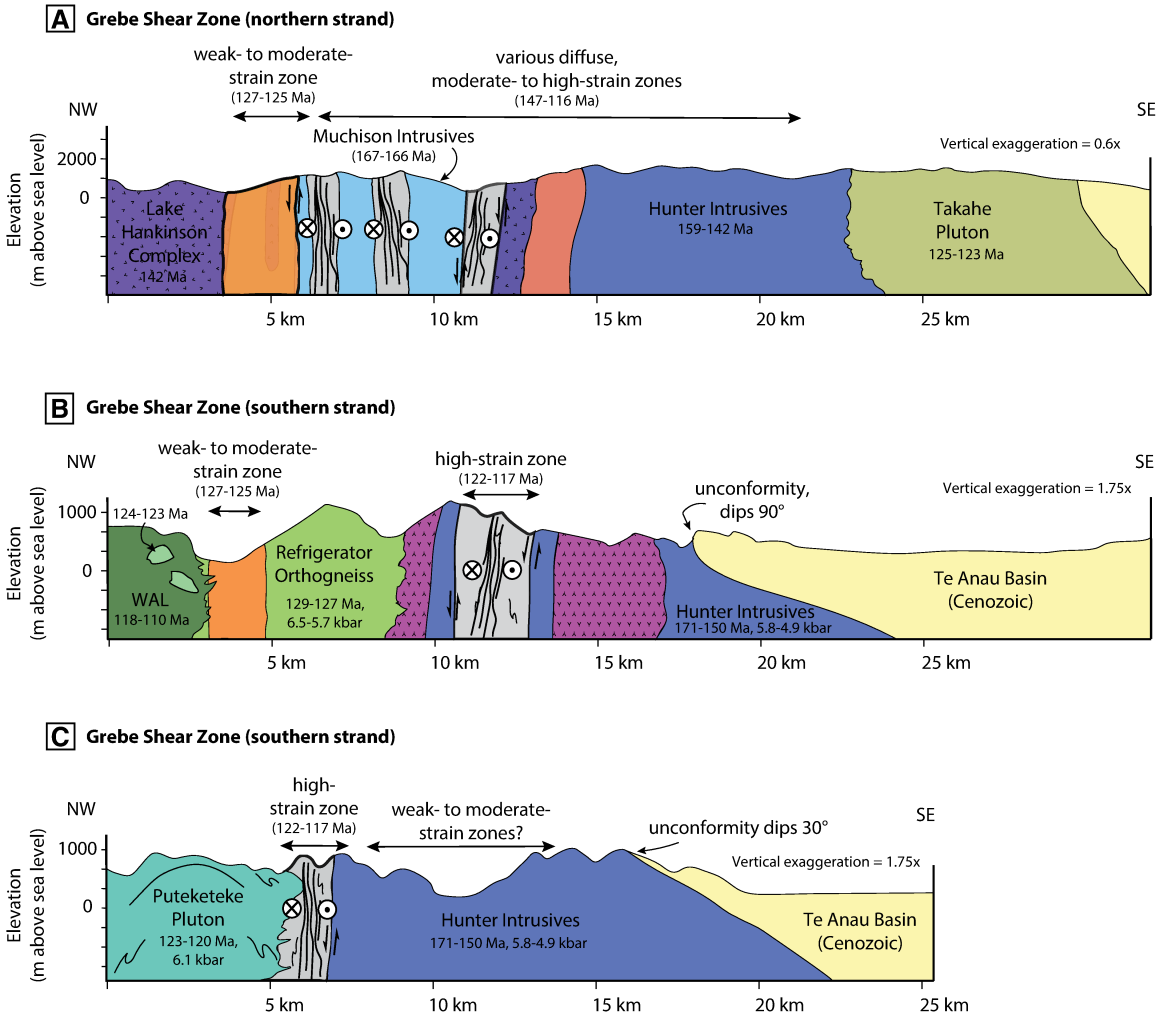

Figure 3. Geologic cross sections of central Fiordland. See Figure 2B for cross-section locations. (A) North shore South Fiord, Lake Te Anau (A–A′). (B) North shore of Lake Manapouri including North Arm (B–B′). (C) South Arm, Lake Manapouri (C–C′). WAL—West Arm Leucogranite.

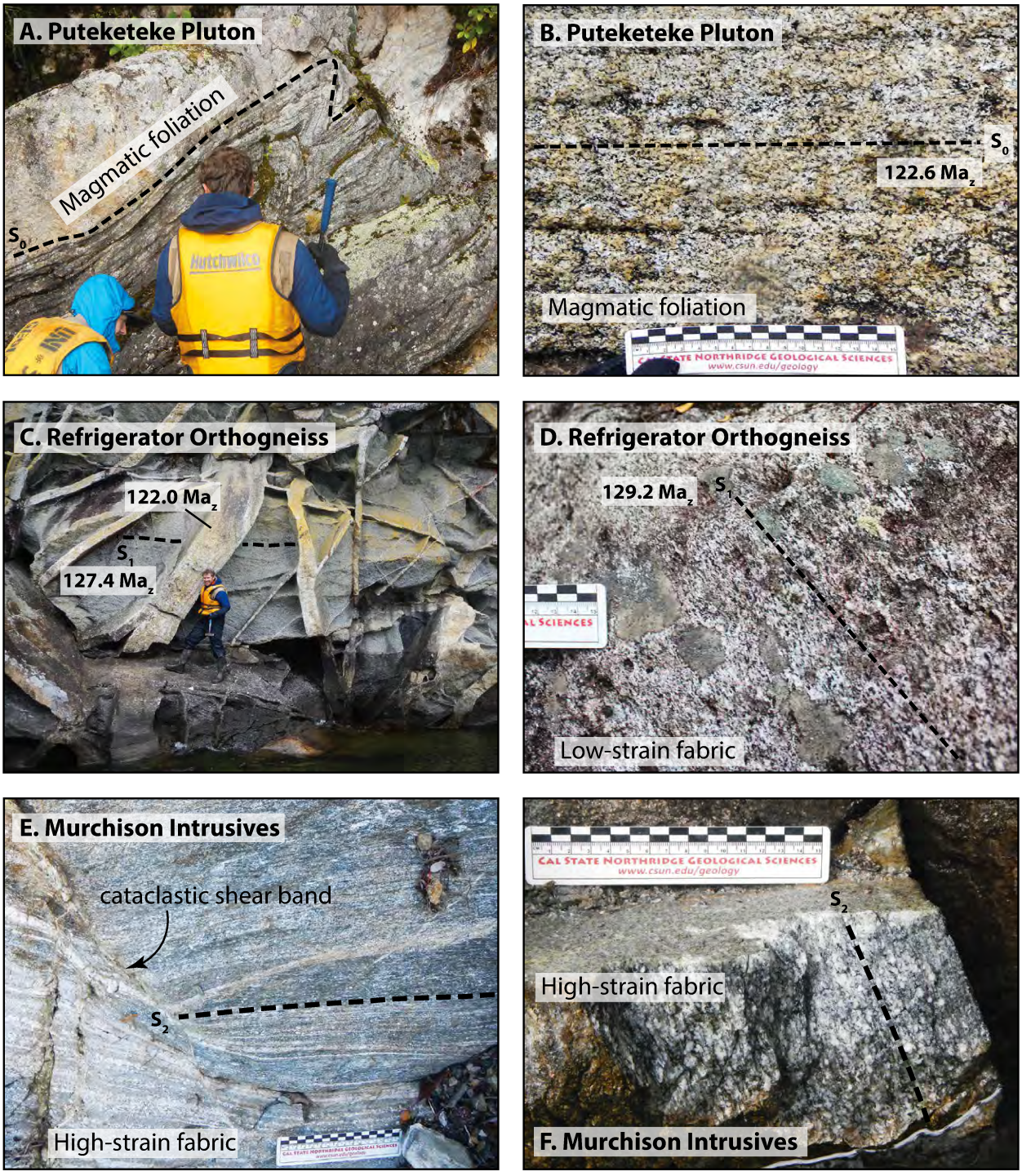

Figure 4. Representative field photographs of structures and corresponding zircon dates where available. (A) Folded magmatic layering in the Puteketeke Pluton (South Arm, Lake Manapouri). (B) Close-up view of weak magmatic layering defined by alignment of biotite, hornblende, and plagioclase (South Arm, Lake Manapouri). Foliation is interpreted to have formed at 122.8 Ma. (C) Weakly foliated, Refrigerator Orthogneiss in low-strain zone cut by various postkinematic dikes (east side of North Arm, Lake Manapouri). The Refrigeration Orthogneiss gave a zircon date of 127.4 Ma, and a crosscutting dike yielded an age of 121.8 Ma, which is similar our dates from the Puteketeke Pluton to the south. (D) Close-up view of low-strain, subsolidus foliation in Refrigerator Orthogneiss defined by alignment of biotite, hornblende, and recrystallized plagioclase. Zircons from this rock yielded an age of 129.1 Ma for the timing of igneous crystallization. (E) Example of a high-strain zone in Murchison intrusives (western South Fiord, Lake Te Anau, north shore). Mylonitic foliation (S2) is defined by recrystallized plagioclase and alignment of biotite and hornblende. Foliation is steeply dipping and is cut by late, greenschist-facies cataclastic shear bands. (F) Close-up view of subvertically dipping, high-strain zone in the Murchison intrusives showing protomylonitic texture defined by aligned biotite, hornblende, and recrystallized plagioclase and quartz (central South Fiord, Lake Te Anau, north shore).

observed no evidence for subsolidus deformation of quartz or plagioclase. Plagioclase laths are commonly oriented parallel to the magmatic fabric.

Low-strain fabrics (S_1 and L_1). These fabrics are defined by more than 50% porphyroclasts, with a fine-grained, recrystallized matrix surrounding larger grains. Low-strain fabrics at the outcrop scale have coarse foliations and weak stretching lineations. Subsolidus foliations (S_1) strike 097°–166° and have dips of 28°–54° southwest (Figs. 4C–4D). Scott et al. (2011) reported that similar foliations in the Refrigerator Orthogneiss and adjacent Lake Hankinson Complex are folded about axes that plunge on average 15° toward 198°. Mineral stretching lineations (L_1) observed in this study are defined by aligned biotite and hornblende and have shallow to moderate southward-trending plunges ranging from 12° to 40° consistent with development during folding. In the Refrigerator Orthogneiss, foliations range from aligned subhedral oligoclase and hornblende laths with little internal strain to more intensely deformed oligoclase and quartz grains. The unstrained fabrics, interpreted by Scott et al. (2011) as hypersolidus fabrics, are overprinted by discontinuous lenses of recrystallized plagioclase and quartz that occur in a matrix of finer-grained biotite, K-feldspar, titanite, and ilmenite (Fig. 4D). Titanite is generally euhedral and lacks evidence for recrystallization (Fig. 5). In contrast, quartz and plagioclase microstructures show evidence for undulose extinction and development of lobate grain boundaries and subgrains. Both weak and more intense subsolidus fabrics are cut by syn- and postkinematic felsic dikes, particularly in North Arm, Lake Manapouri (Fig. 4C).

High-strain fabrics (S_2 and L_2). These fabrics were identified in mylonitic rocks in Lake Manapouri, and in schists, gneisses, and mylonites in South Fiord of Lake Te Anau (Figs. 4E–4F). We collectively refer to the fabrics as the "Lake Manapouri mylonites" and the "Lake Te Anau mylonites," though they include schistose, gneissic, mylonitic, and ultramylonitic fabrics. These higher-intensity fabrics contrast with the weak, subsolidus deformational fabrics that characterize the Refrigerator Orthogneiss (cf. Fig. 4D vs. Figs. 4E–4F). In general, higher-strain fabrics are moderately to steeply dipping and parallel the overall trend of the Median Batholith. In South Fiord, Lake Te Anau, high-strain fabrics occur over an ~20-km-wide zone and display north-striking and moderately to steeply west-dipping (45°–84°) S_2 foliations with moderately (47°–64°) southwest-plunging L_2 mineral lineations. S_2 foliations occur throughout all rocks mapped as Darran Suite on the north shore of South Fiord, including the Lake Hankinson Complex and the Hunter and Murchison intrusives. No high-strain zones were observed in the Takahe Pluton, located at the far east end of South Fiord. S_2 fabrics in the Darran Suite are typically defined by clusters of plagioclase, quartz, biotite, hornblende, and minor anhedral titanite. At the boundary between the Hunter and Murchison intrusives, deformation is focused into a distributed, ~3-km-wide shear zone, which contains several discrete high-strain zones that grade from mylonite to ultramylonite (Figs. 2B and 3; McGinn, 2018). Mylonitic foliations in this shear zone primarily strike NE-SW and dip moderately to steeply SW. Mineral stretching lineations plunge moderately toward the S-SW and steepen from west to east in the shear zone (McGinn, 2018). In this zone, high-strain mylonites are particularly well developed in muscovite- and biotite-bearing granitic gneisses that contain conspicuous rutilated quartz.

In Lake Manapouri, high-strain fabrics also occur in granitic gneisses in South Arm, some of which contain rutilated quartz, along with biotite and plagioclase, with trace amounts of apatite, muscovite, epidote, and

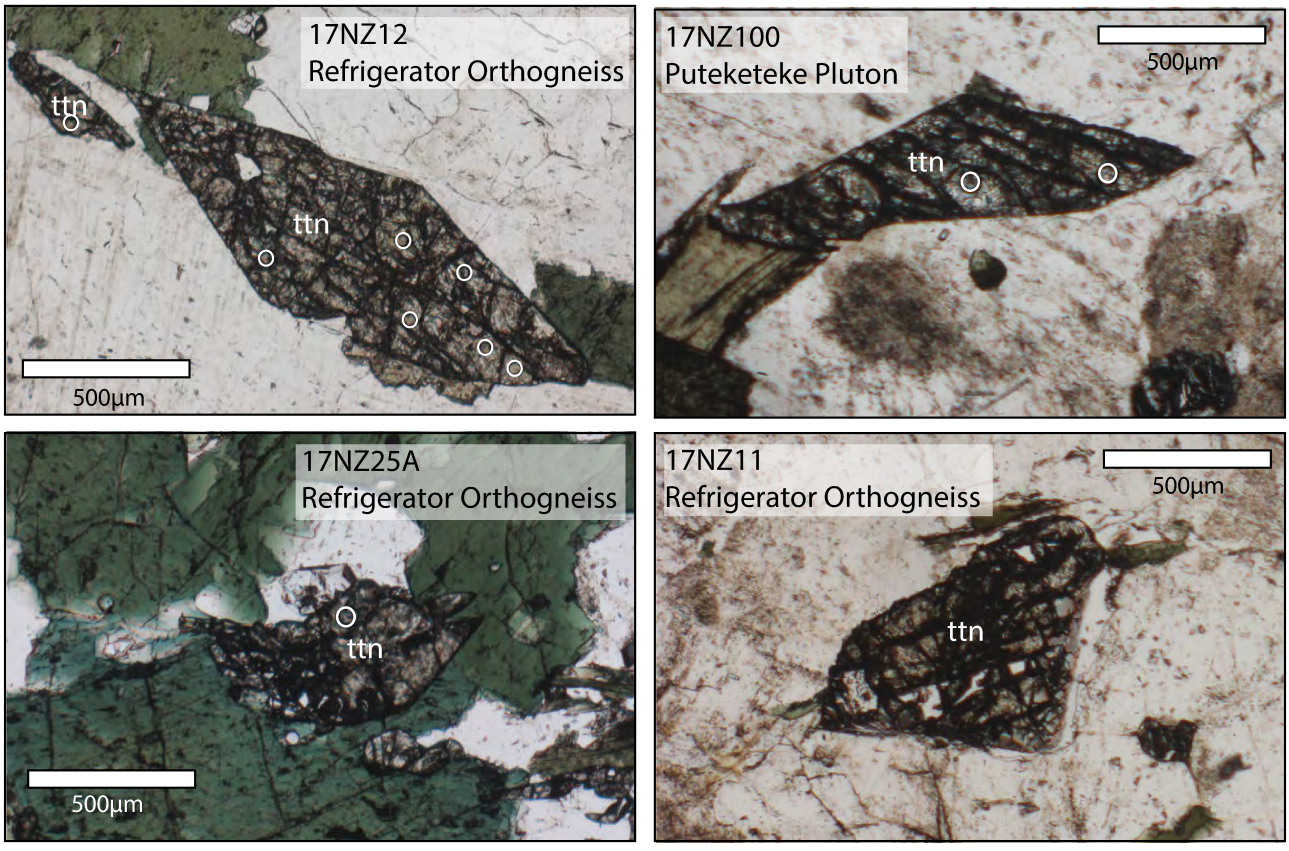

Figure 5. Representative plane-polarized light images of type I titanites. Samples are from Refrigerator Orthogneiss (low-strain fabrics) and Puteketeke Pluton (magmatic fabrics); ttn—titanite. White circles are laser-ablation spots.

zircon. Gneisses in this region are composed of alternating layers of feldspar-rich and polycrystalline quartz bands. Foliations are typically defined by biotite and elongate plagioclase. Quartz occurs as anastomosing, interconnected bands in some samples. Quartz microstructures show undulose extinction and lobate grain boundaries. Plagioclase generally lacks obvious evidence for recrystallization. Sigma porphyroclasts of plagioclase and potassium feldspar generally display sinistral shear (three out of five field stations), although dextral shear sense was also observed. In thin section, mica fish also give a sinistral sense of shear, which is consistent with previous interpretations of the sinistral transpressional deformation in this zone and to the north (Marcotte et al., 2005; Scott et al., 2011).

Northern Fiordland

Cretaceous deformational fabrics are recorded in several ductile shear zones in northern Fiordland and include from west to east: the George Sound shear zone, the Mount Daniel shear zone, and the Indecision Creek shear zone (Klepeis and Clarke, 2004; Klepeis et al., 2004; Marcotte et al., 2005). Here, we focus on the latter two shear zones and their relationship to deformation in central Fiordland (Fig. 2A). The Indecision Creek shear zone is a N-S–striking ductile shear zone that occurs within Darran Suite rocks and the Arthur River Complex. Klepeis et al. (2004) and Marcotte et al. (2005) described the fabric evolution of the Indecision Creek shear zone and the development of triclinic, partitioned transpression involving dip-slip and oblique-slip displacements. Transpressional fabrics in the Indecision Creek shear zone occur over a ~20-km-wide zone where deformation is partitioned into structural domains distinguished based on structure style and the orientation of rock fabrics through time (Marcotte et al., 2005). Magmatic and solid-state fabrics include: (1) gneissic and igneous layering in the Worsley Pluton and Mount Edgar Diorite (domain i: Mount Daniel shear zone), (2) polyphase fabrics and folding in the Arthur River Complex (domain ii: western margin of the Indecision Creek shear zone), and (3) steeply foliated fabrics associated with tight folds, mylonitic shear zones, and syntectonic dikes (domain iii: core of the Indecision Creek shear zone). Here, we focus on fabrics developed in domains i and ii (Mount Daniel and western Indecision Creek shear zones).

In domain i, ductile shear fabrics associated with the Mount Daniel shear zone (Fig. 2A) occur at the boundary between the Worsley Pluton (hanging wall) and Arthur River Complex (footwall). Early gneissic layering in this region is characterized by moderate to high strains associated with south- and southwest-dipping fabrics (S_1) that formed at high temperatures during magmatic emplacement of the Worsley Pluton. These early magmatic fabrics are deformed by a moderate, penetrative, subsolidus south- to southwest-dipping foliation (S_2) that is defined by flattened clusters of upper-amphibolite-facies mineral assemblages including plagioclase, quartz, biotite, hornblende, and garnet. We collected two samples from this region, which record an early high-strain fabric (0308F), and a later moderate-strain fabric (0308L1; Table 2).

In domain ii, polyphase folding is preserved at Steep Hill, along the western margin of the Indecision Creek shear zone (domain ii of Marcotte et al., 2005). Here, the Arthur River Complex consists of gneissic gabbros and diorites of the Milford Gneiss, which are cut by mafic dikes. Early high-grade, gneissic layering (S_1) and dikes are transposed parallel to a penetrative gneissic foliation (S_2). Foliations associated with this fabric generally strike E-W and dip moderately to the south. Garnet + plagioclase + quartz leucosomes developed in migmatitic gneisses parallel S_2 foliations, and mineral lineations plunge moderately to the north, south, and southwest. S_2 foliations are overprinted by a series of upright, northwest-verging folds and steeply dipping foliations (S_3) that characterize higher-strain zones to the east in the core of the Indecision Creek shear zone. Our sample (0213K1) from this area is a retrogressed (schistose) mafic gneiss from the early high-grade fabric (S_2; Table 2). Textures related to the early, high-grade fabric include large garnet porphyroblasts in a migmatite gneissic fabric with biotite and plagioclase pressure shadows.

Titanite Petrographic Observations and Relationships to Fabrics

Petrographic analysis indicated that titanite occurs in two textural categories in northern and central Fiordland, which we define as type I and type II titanites (Figs. 5–6). We defined these two groups based on their morphology, grain size, and textural and mineral relationships within the host rock. They are also distinguished based on geochemistry (see below).

Type I Titanites (Aligned in S_0 and S_1 Fabrics): Euhedral to Subhedral Grains

Type I titanites consist of euhedral to subhedral morphologies and occur primarily in foliated magmatic fabrics in the Puteketeke Pluton and in weakly foliated, subsolidus fabrics in the Refrigerator Orthogneiss (Fig. 5). Titanite grains have average lengths of 400–800 µm. Crystals are generally yellow brown to dark brown. Some titanite grains show weak internal zoning in BSE imaging. Type I titanites are generally aligned in S_0 and S_1 fabrics.

Type II Titanites (Aligned in S_2 Fabrics): Anhedral Grains and Aggregates

Type II titanites are typically represented by clusters of anhedral aggregates with subhedral individual grains (Fig. 6). Titanite grains are on average 100–400 µm long. Crystals are yellow brown to dark brown. Some titanite grains also display minor internal zoning in BSE imaging (Fig. 7). Crystals with inclusions of oxides (e.g., magnetite, ilmenite) are common. Titanite grains are oriented parallel to foliation and are found in samples with upper- to middle-amphibolite-facies mylonitic fabrics in Lake Manapouri and Lake Te Anau mylonites, the Indecision Creek shear zone, and the Mount Daniel shear zone.

Titanite LA-MC-ICP-MS Geochronology

Type I and II titanites were dated from plutonic and metamorphic rocks in order to constrain the timing of titanite growth and deformation. Examples of titanite BSE images and LASS spot analysis locations are shown in Figure 7. Concordia diagrams with lower-intercept regressions are given in Figure 8. Data are summarized in Table 3, and full data sets are given in the GSA Data Repository Item.[1]

Type I Titanites (Aligned in S_0 and S_1 Fabrics)

Puteketeke Pluton (magmatic fabric S_0). Two samples (17NZ100, 17NZ104) from Puteketeke Pluton contain titanite grains that defined weak igneous layering with oriented biotite. Titanite grains in samples 17NZ100 and 17NZ104 yielded $^{206}Pb/^{238}U$ lower-intercept ages of 118.4 ± 1.3 Ma (mean square of weighted deviates [MSWD] = 0.8) and 115.7 ± 1.4 Ma (MSWD = 1.5), respectively (Figs. 8A and 8B). Our titanite ages overlap within error of a lower-intercept date of 113.7 ± 7.3 Ma reported by Scott et al. (2009).

Refrigerator Orthogneiss (low-strain fabric S_1). Samples from the Refrigerator Orthogneiss (17NZ12, 17NZ11, 17NZ124A, 17NZ25A) contain titanite grains with average diameter between 100 and 200 µm and

[1]GSA Data Repository Item 2019309, U-Pb zircon and titanite isotope data, and titanite geochemistry data, is available at http://www.geosociety.org/datarepository/2019, or on request from editing@geosociety.org.

TABLE 2. SAMPLE LOCATIONS AND PETROGRAPHIC DESCRIPTIONS.

Sample	Unit	Rock type	Description	Mineral assemblages	Location
17NZ4A	Lake Hankinson Complex	bt gneiss	Moderate to strong schistose foliation. Host of a postkinematic felsic dike.	qz, plg, bt, hbl, ttn, zrn, czo	South Fiord, Lake Te Anau
17NZ11	Refrigerator Orthogneiss	hbl-bt tonalite	Moderate foliation S_1. Low strain. Ttn aligned with S_1.	plg, qz, kfs, qz, bt, hbl, ttn, ap, zrn, opq	South Fiord, Lake Te Anau
17NZ12	Refrigerator Orthogneiss	hbl-bt tonalite	Moderate foliation S_1. Low strain. Ttn aligned with S_1.	plg, qz, kfs, qz, bt, hbl, ap, ttn, zrn, opq	South Fiord, Lake Te Anau
17NZ25A	Refrigerator Orthogneiss	hbl-bt tonalite	Moderate foliation S_1. Low strain. Ttn aligned with S_1. Localized anastomosing bands of qz-plg.	plg, qz, kfs, qz, bt, hbl, ttn, ap, zrn, opq	South Fiord, Lake Te Anau
17NZ25B	Refrigerator Orthogneiss	pegmatite dike (postkinematic)	Postkinematic dike. Cuts fabric in host.	plg, kfs, qz, zrn	South Fiord, Lake Te Anau
17NZ31A	Murchison intrusives	hbl diorite gneiss	Moderate to strong foliation S_2. High strain. Fine-grained hbl diorite.	plg, qz, hbl, chl, czo, ttn, opq	South Fiord, Lake Te Anau
17NZ31B	Murchison intrusives	granitic dike (synkinematic)	Synkinematic dike. Oriented semiparallel to the mylonitic fabric in host.	plg, kfs, qz, zrn	South Fiord, Lake Te Anau
17NZ40	Murchison intrusives	diorite mylonite	Moderate to strong foliation S_2. High-strain. Fine-grained diorite. Chl and ser as secondary minerals.	plg, qz, hbl, chl, czo zrn, opq, ser	South Fiord, Lake Te Anau
17NZ43A	Murchison intrusives	diorite mylonite	Moderate to strong foliation S_2. High strain. Mylonite medium-grained. Ttn aligned in fabric.	plg, qz, hbl, chl, czo, ap, ttn, opq	South Fiord, Lake Te Anau
17NZ43B	Murchison intrusives	pegmatite dike (postkinematic)	Postkinematic dike. Cuts fabric in host.	hbl, bt, ttn, zrn, czo	South Fiord, Lake Te Anau
17NZ44	Hunter intrusives	granite	Moderate foliation S_2. Moderate to high strain.	plg, qz, hbl, chl, czo zrn, opq	South Fiord, Lake Te Anau
17NZ55A	Hunter intrusives	hbl-bt tonalite mylonite	Strong S_2 foliation. Medium-coarse tonalite. High-strain mylonite. Chl and ser as secondary minerals. Ttn aligned with S_2.	qz, plg, hbl, bt, ttn, czo, chl, ser	South Fiord, Lake Te Anau
17NZ60	Hunter intrusives	hbl diorite mylonite	Strong S_2 foliation. High strain. Medium-coarse diorite mylonite. Ttn aligned with S_2.	plg, hbl, bt, qz, ttn	South Fiord, Lake Te Anau
17NZ72A	Hunter intrusives	hbl diorite protomylonite	Weak to moderate S_2 foliation. Fine-grained protomylonite. Ttn aligned with S_2.	plg, qz, hbl, bt, ttn, czo	South Fiord, Lake Te Anau
17NZ78B	Takahe Granodiorite	bt granodiorite	Undeformed bt granodiorite.	plg, kfs, qz, bt, white mica, ap, zrn, opq	South Fiord, Lake Te Anau
17NZ81	Takahe Granodiorite	bt granodiorite	Undeformed bt granodiorite.	plg, kfs, qz, bt, white mica, ap, zrn, opq	South Fiord, Lake Te Anau
17NZ94	Lake Manapouri mylonite	bt-hbl diorite mylonite	Moderate foliation S_2. High strain. Ttn aligned with S_2. Localized anastomosing bands of qz-plg.	plg, qz, bt, hbl, chl, czo zrn, opq	South Arm, Lake Manapouri
17NZ95B	Lake Manapouri mylonite	hbl-bt diorite mylonite	Strong S_2 foliation. High strain. Medium-grained diorite mylonite. Quartz-rich band. Ttn aligned with S_2.	plg, qz, hbl, bt, ttn, opq, zrn, czo	South Arm, Lake Manapouri
17NZ96	Lake Manapouri mylonite	bt diorite mylonite	Strong S_2 foliation. High strain. Fine-grained hbl diorite mylonite. Ttn-rich band. Ttn aligned with S_2.	plg, qz, bt, hbl, ttn, zrn, ap, czo, ser	South Arm, Lake Manapouri
17NZ98	Puteketeke Pluton	bt granodiorite	Weak S_0 foliation. Bt-granodiorite with weak magmatic foliation.	plg, kfs, qz, bt, ap, zrn, opq	South Arm, Lake Manapouri
17NZ100	Puteketeke Pluton	bt tonalite	Weak S_0 foliation. Bt-granodiorite with magmatic foliation (alignment of bt). Moderate alignment of ttn.	plg, kfs, qz, bt, ap, ttn, zrn, opq	South Arm, Lake Manapouri
17NZ104	Puteketeke Pluton	bt tonalite	Weak S_0 foliation. Coarse-grained bt-tonalite.	plg, kfs, qz, bt, ap, ttn, zrn, opq	South Arm, Lake Manapouri
17NZ114	West Arm Leucogranite	hbl-bt tonalite	Weak fabric S_1 defined by alignment of bt.	plg, kfs, qz, bt, czo, ttn, zrn, ap, opq	West Arm, Lake Manapouri
17NZ117	West Arm Leucogranite	bt granodiorite	Undeformed bt granodiorite.	plg, kfs, qz, bt, zrn, opq, ap	West Arm, Lake Manapouri
17NZ124A	Refrigerator Orthogneiss	bt tonalite	Undeformed bt tonalite.	plg, qz, bt, hbl, chl, czo zrn, opq	West Arm, Lake Manapouri
17NZ124B	Refrigerator Orthogneiss	pegmatite dike (postkinematic)	Postkinematic dike. Cuts fabric in host.	plg, kfs, qz, bt, zrn, opq, ap	West Arm, Lake Manapouri
17NZ127	Refrigerator Orthogneiss	pegmatite dike (postkinematic)	Undeformed bt granitic dike.	plg, kfs, qz, bt, opq, ttn, ap, zrn	West Arm, Lake Manapouri
17NZ134	West Arm Leucogranite	bt tonalite	Undeformed bt tonalite.	plg, kfs, qz, bt, zrn, opq	North Arm, Lake Manapouri
17NZ137	West Arm Leucogranite	bt tonalite	Undeformed bt tonalite.	plg, kfs, qz, bt, zrn, opq	North Arm, Lake Manapouri
17NZ139	West Arm Leucogranite	bt granite	Undeformed bt granite.	plg, kfs, qz, bt, white mica, zrn, opq, ap	Percy Saddle
17NZ140	West Arm Leucogranite	bt granodiorite	Undeformed bt granodiorite.	plg, kfs, qz, bt, white mica, zrn, opq, ap	Percy Saddle
17NZ141	West Arm Leucogranite	granodiorite	Undeformed granodiorite.	plg, kfs, qz, ms, zrn, opq, ap	Percy Saddle
0213K1	Indecision Creek shear zone	grt diorite gneiss	High-strain grt diorite gneiss.	grt, plg, qz, cpx, bt, ttn, opq	Steep Hill
0308F	Mount Daniel shear zone	grt diorite gneiss	High-strain gneiss.	plg, qz, hbl, grt, ttn, czo, opq	Mount Daniel
0308L1	Mount Daniel shear zone	bt diorite schist	Low-to-moderate strain bt schist.	plg, czo, bt, hbl, ttn, opq	Mount Daniel

Note: Mineral abbreviations are after Whitney and Evans (2010): ap—apatite; bt—biotite; chl—chlorite; cpx—clinopyroxene; czo—clinozoisite; grt—garnet; hbl—hornblende; kfs—k-feldspar; opq—opaque mineral; plg—plagioclase; qz—quartz; ser—sericite; ttn—titanite; zrn—zircon. Unit names follow Turnbull et al. (2010).

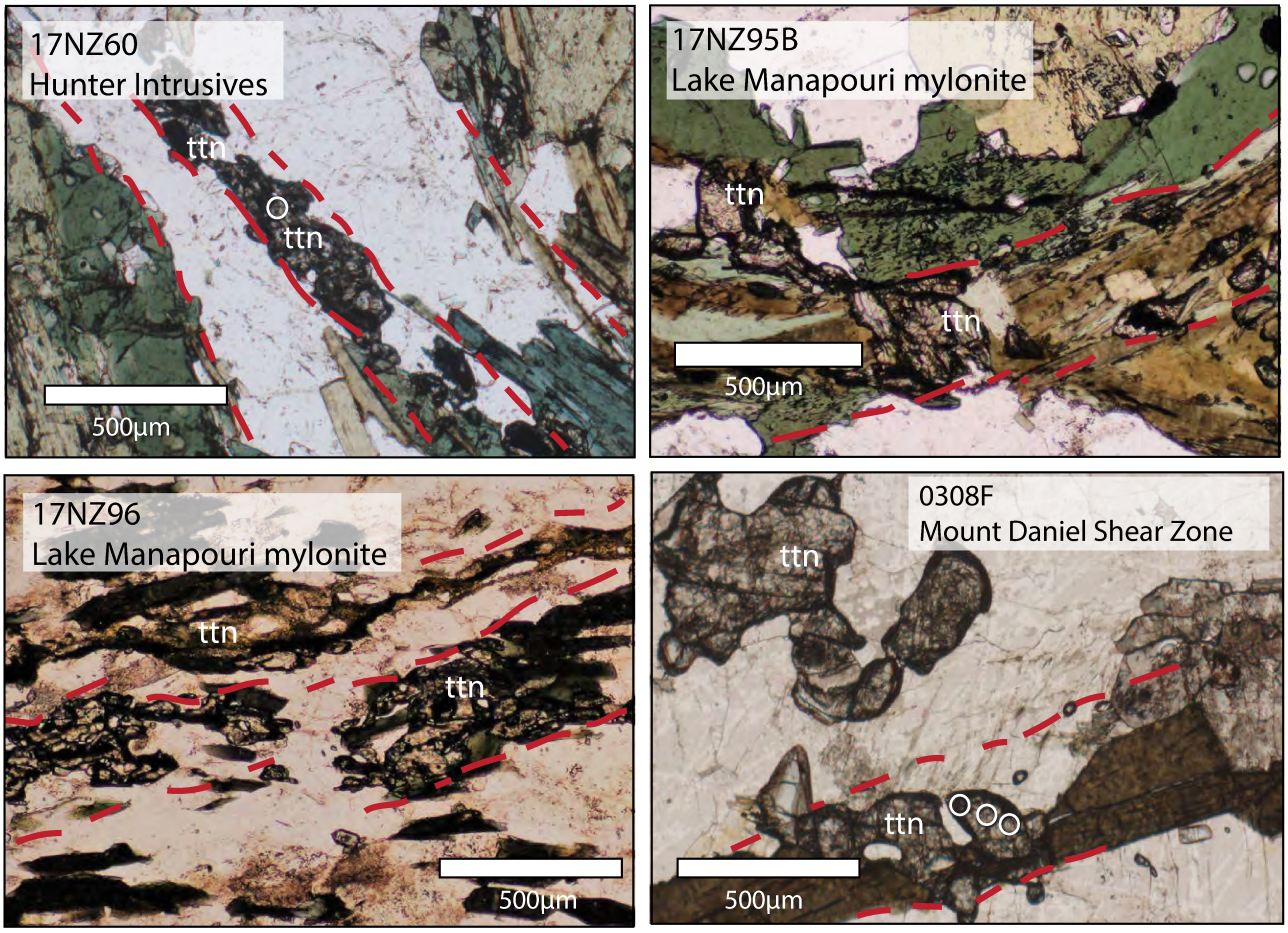

Figure 6. Representative plane-polarized light images of type II titanites. Samples are from Hunter intrusives, Lake Manapouri mylonites, and the Mount Daniel shear zone; ttn—titanite. White circles are laser-ablation spots.

lower-intercept dates clustering at 122–117 Ma (Figs. 8C–8F). Seventy-seven titanite grains from sample 17NZ12 plot along a discordia array with a large MSWD (7.6), indicating greater scatter than can be accounted for by analytical uncertainties alone. Anchoring of the upper intercepts at $^{207}Pb/^{206}Pb$ = 0.80 and 0.72 produces two discordia arrays with lower-intercept ages of 120.3 ± 0.4 Ma (MSWD = 7.6) and 118.3 ± 0.4 Ma (MSWD = 7.6), respectively. Titanites from sample 17NZ11 yielded a single discordia array with a lower-intercept $^{206}Pb/^{238}U$ age of 121.4 ± 1.4 Ma (MSWD = 1.2) from 28 spots. Analyses from sample 17NZ124A plot along a discordia array (48 spots) with a lower-intercept $^{206}Pb/^{238}U$ age of 117.3 ± 0.8 Ma (MSWD = 1.6). Seventy-two titanite grains from sample 17NZ25A plot along a discordia array with a lower-intercept $^{206}Pb/^{238}U$ age of 120.8 ± 1.5 Ma (MSWD = 0.8). Scott et al. (2009) reported a lower-intercept date of 120.7 ± 3.1 Ma, which lies within error of our ages reported here.

Type II Titanites (Aligned in S_2 Fabrics)

Lake Manapouri mylonites. Two samples (17NZ95B, 17NZ96) were collected from high-strain zones in South Arm, Lake Manapouri. Titanite grains from these samples show average diameters between 300 and 400 µm and form anhedral aggregates aligned with the fabric S_2 (Fig. 6). Forty titanite grains from sample 17NZ95B yielded a lower-intercept $^{206}Pb/^{238}U$ age of 117.1 ± 3.2 Ma (MSWD = 2.3; Fig. 8G). This sample contains an inherited Pb component (or composition) that defines an older population with a lower-intercept $^{206}Pb/^{238}U$ age of 307.7 ± 3.7 Ma and MSWD = 28. Eighteen titanite grains from sample 17NZ96 plot along a discordia array with a lower-intercept $^{206}Pb/^{238}U$ age of 122.3 ± 1.8 Ma (MSWD = 2.3; Fig. 8H). This sample also contains a poorly defined older population.

Lake Te Anau mylonites. Six samples (17NZ43A, 17NZ60, 17NZ55A, 17NZ72A, 17NZ31A, 17NZ4A) were collected in South Fiord, Lake Te Anau, where series of diffuse high-strain, gneissic to mylonitic shear zones were identified. Based on our U-Pb zircon data (see below), these diffuse shear zones are hosted in Carboniferous and Jurassic dioritic rocks. Sample 17NZ43A yielded a lower-intercept $^{206}Pb/^{238}U$ age of 123.2 ± 9.6 Ma (MSWD = 0.4) from 29 spots (Fig. 8I). Twenty-eight analyses from sample 17NZ60 form a discordia array with a lower-intercept $^{206}Pb/^{238}U$ date of 116.3 ± 1.7 Ma (MSWD = 0.4; Fig. 8J). Titanite grains from sample 17NZ31A yielded a titanite $^{206}Pb/^{238}U$ date of 125.7 ± 7.4 Ma (MSWD = 0.6) from 37 grains (Fig. 8K). Forty titanite analyses from sample 17NZ4A plot along a discordia array with a lower-intercept $^{206}Pb/^{238}U$ date of 125.3 ± 1.4 Ma (MSWD = 4.2; Fig. 8L). Thirty-four analyses from sample 17NZ55A plot along a discordia array with a lower-intercept $^{206}Pb/^{238}U$ date of 146.8 ± 2.3 Ma (MSWD = 2.4; Fig. 8M). Sixty-six spots in sample 17NZ72A yielded a lower-intercept $^{206}Pb/^{238}U$ age of 130.8 ± 1.8 Ma (MSWD = 1.1; Fig. 8N).

Indecision Creek and Mount Daniel shear zones (northern Fiordland). Thirty spots from sample 2013K1 from the western margin of the Indecision Creek shear zone (Fig. 2A) yielded a lower-intercept $^{206}Pb/^{238}U$

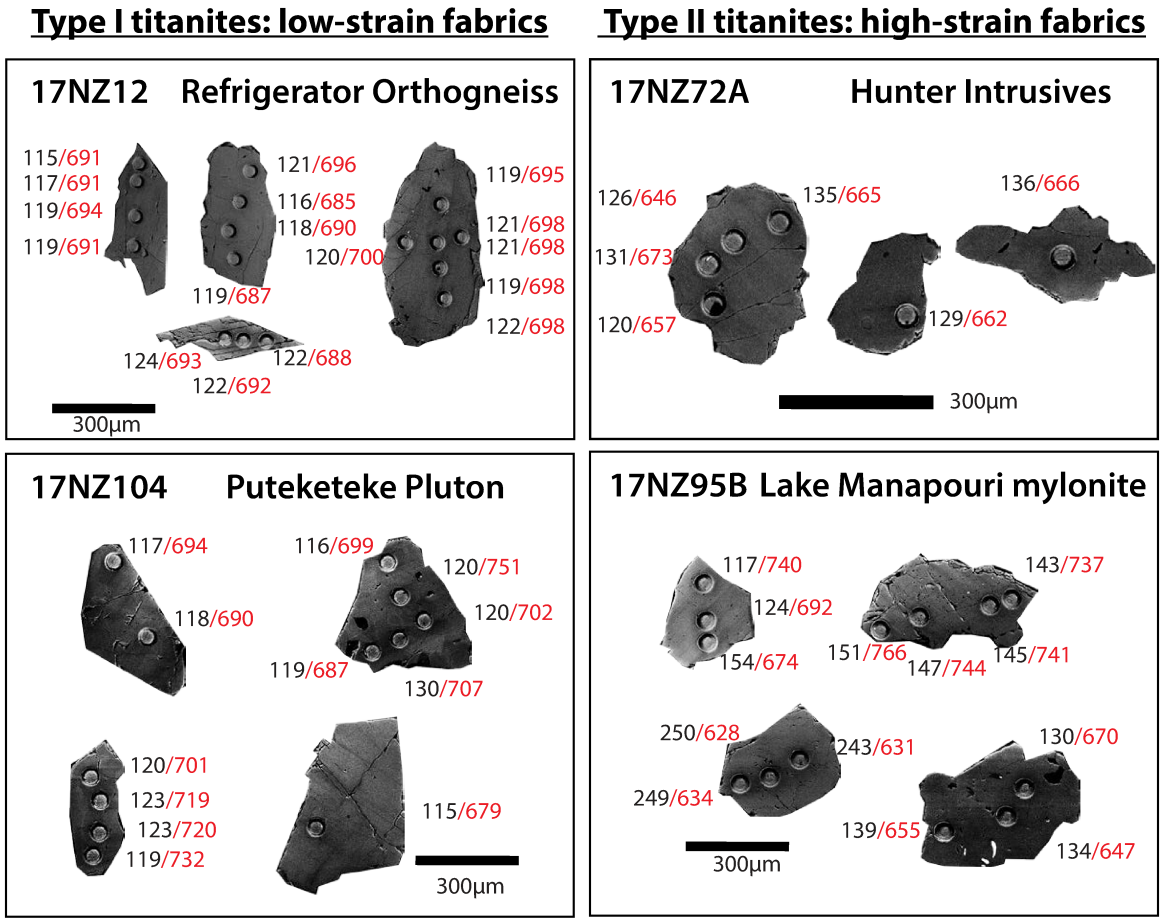

Figure 7. Backscattered electron images of representative titanite grains with individual spots. Black numbers represent common Pb–corrected $^{206}Pb/^{238}U$ dates (Ma), and red numbers represent model temperatures (°C) calculated using the pressure-dependent zirconium-in-titanite thermometer of Hayden et al. (2008).

age of 119.8 ± 2.0 Ma (MSWD = 5.9; Fig. 8O). Eight spots with high common Pb and low radiogenic Pb values were excluded because they do not lie along the same discordia array. From the Mount Daniel shear zone, 42 spots from sample 0308F plot along a discordia array with a lower-intercept $^{206}Pb/^{238}U$ date of 111.1 ± 1.2 Ma (MSWD = 0.7; Fig. 8P). One analysis yielded a younger date and was excluded from this array. Sample 0308L1 spots plot along a discordia array (30 analyses) with a lower-intercept $^{206}Pb/^{238}U$ date of 105.5 ± 3.6 Ma (MSWD = 1.1; Fig. 8Q).

Titanite Geochemistry and Thermometry

Titanite trace-element geochemical data show that titanite grains form two distinct groups that correlate with microscopic textures (Figs. 9A–9F). Type I titanites are distinguished by enrichment in light rare earth elements/heavy rare earth elements (LREEs/HREEs), whereas type II titanites display a distinctive depletion in LREE/HREE (cf. Fig. 9A and 9D). Type I samples generally have either weak positive or negative europium (Eu) anomaly, and type II titanites consistently have no Eu anomaly ($Eu/Eu^* = \sqrt{Sm \times Gd}$). In general, type I titanites display a positive correlation between temperature and La concentrations, reflecting fractional crystallization processes (Fig. 9B). Type I titanites also generally exhibit a broad intrasample Zr-in-titanite temperature range (50–150 °C) and give sample-average temperatures ranging from ~675 °C to 700 °C, with 1σ standard deviations ranging from 4 °C to 7 °C (Figs. 9B–9C; Table 3). Type II titanites generally show a more restricted intrasample temperature range (~50–100 °C) and give overlapping to somewhat lower sample-average temperatures ranging from ~610 °C to 700 °C, with 1σ standard deviations ranging from 4 °C to 8 °C (Figs. 9E–9F; Table 3). Compared to type I titanites, type II titanites have much lower La concentrations and La/Sm values (cf. Figs. 9B–9C with Fig. 9E–9F).

Zircon SHRIMP-RG Geochronology

Separation Point Suite

Zircon crystallization ages from five plutons in central Fiordland were determined in order to constrain the timing of Separation Point Suite magmatism associated with the high-magma-addition-rate event. In some instances, postkinematic dikes were dated to place minimum time constraints on the timing of subsolidus deformation. Examples of zircon cathodoluminescence images and SHRIMP-RG spot analysis locations are shown in Figure 10. Concordia diagrams are given in Figure 11. Data are summarized in Table 4 and in the Data Repository.

Refrigerator Orthogneiss

Three tonalitic samples were collected from the Refrigerator Orthogneiss (17NZ12, 17NZ25A, 17NZ124A) in Lake Te Anau and Lake

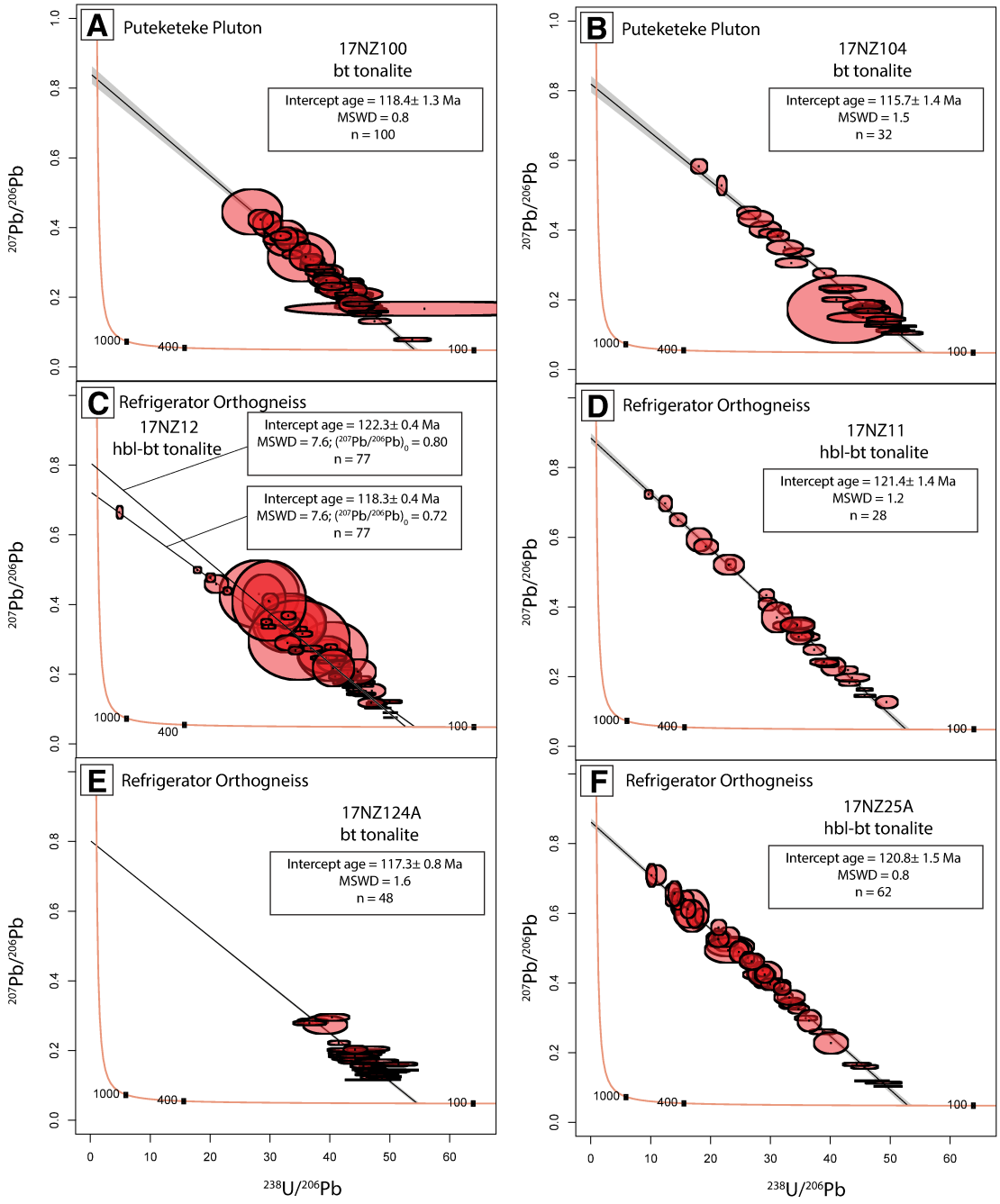

Figure 8. Tera-Wasserburg concordia diagrams showing titanite data. Concordia diagrams show all spots (including rejected spots in white). Error ellipses are shown at 2σ total uncertainty for spot analyses. MSWD—mean square of weighted deviates; bt—biotite; hbl—hornblende; grt—garnet. (*Continued on following page.*)

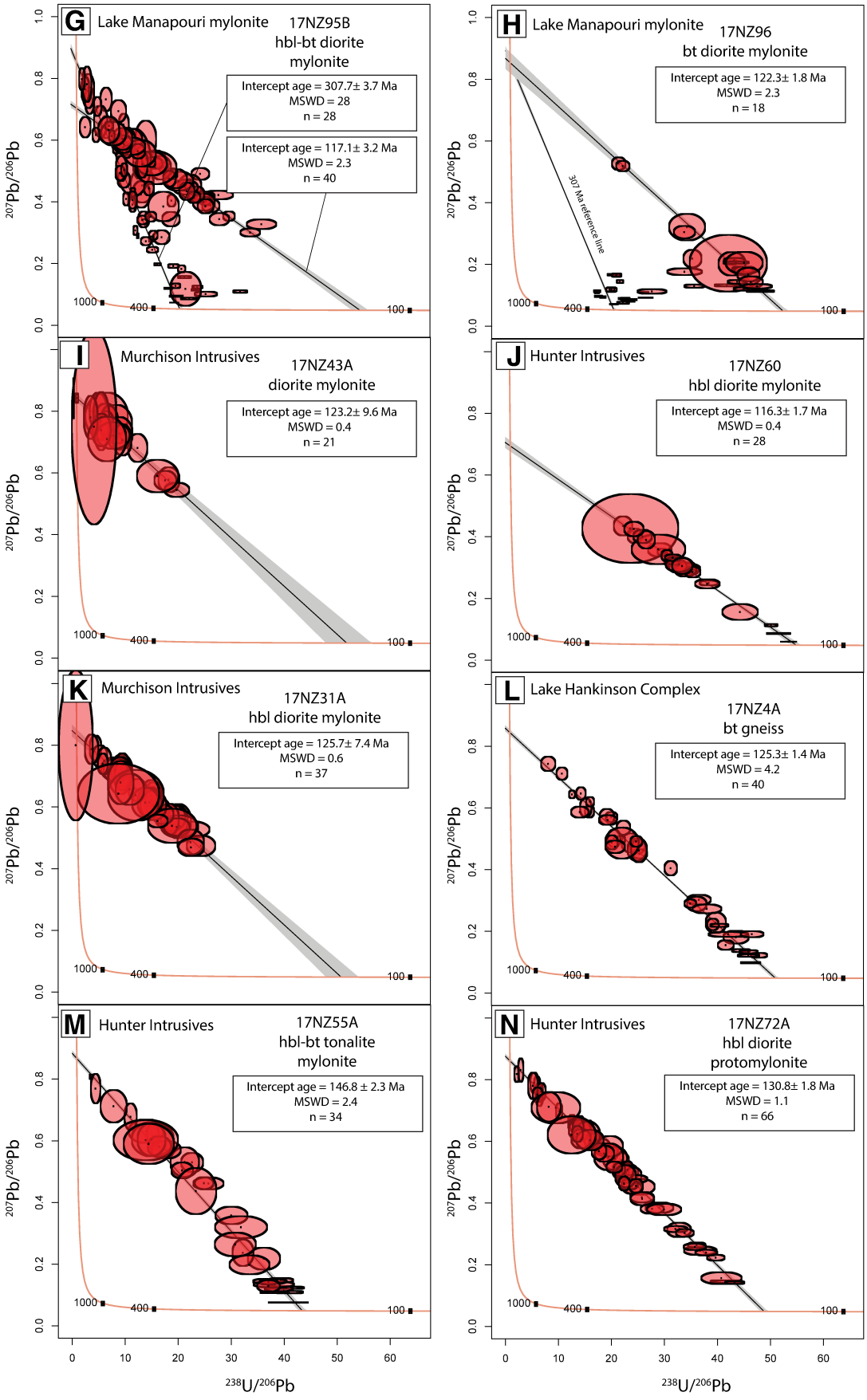

Figure 8 (*continued*).

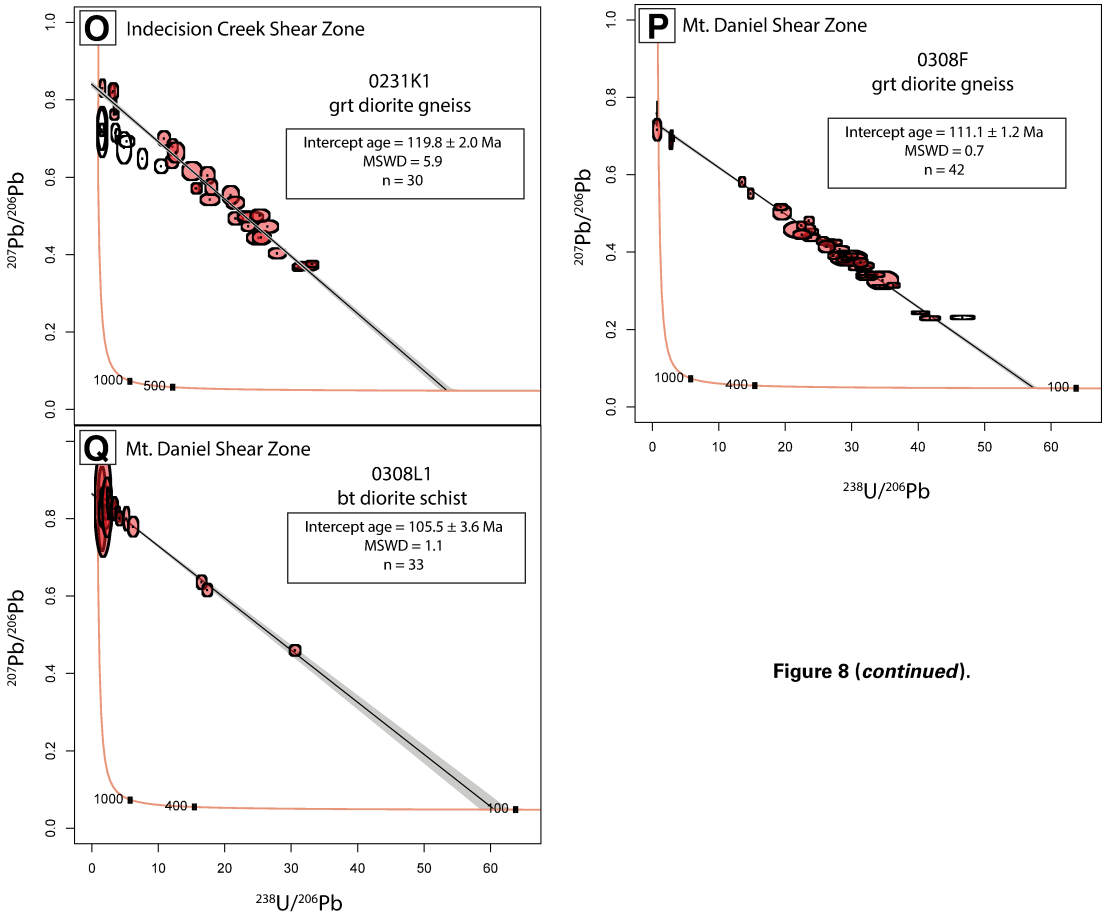

Figure 8 (*continued*).

Manapouri. Zircon grains display average diameters between 50 and 150 µm and aspect ratios of 1:1–1:2, with subhedral to euhedral crystal habit and a few low-U rims. Sample 17NZ12 yielded an error-weighted average date of 128.8 ± 1.7 Ma (MSWD = 2.8) from 10 individual zircon analyses (Fig. 11A), excluding one statistically younger date (117 Ma). Eight spots from sample 17NZ25A were analyzed and yielded an error-weighted average $^{206}Pb/^{238}U$ date of 129.2 ± 1.7 Ma (MSWD = 0.8; Fig. 11B). Sample 17NZ124A (n = 10) yielded an error-weighted average $^{206}Pb/^{238}U$ date of 127.4 ± 1.3 Ma (MSWD = 2.0; Figs. 10 and 11C).

Zircons from three post-S_1 pegmatite dikes (17NZ127, 17NZ25B, 17NZ124B) display subhedral to euhedral crystal habit, chaotic patchy zoning, and low-U domains. From sample 17NZ127, seven spots yielded an error-weighted average $^{206}Pb/^{238}U$ date of 112.7 ± 1.3 (MSWD = 1.2; Fig. 11D). Two xenocrystic zircons giving ages of 128–122 Ma were excluded. Sample 17NZ25B yielded an error-weighted average $^{206}Pb/^{238}U$ date of 124.1 ± 1.4 (MSWD = 2.8) from seven spots analyzed (Fig. 11E). One statistically younger spot (116 Ma) was excluded in the weighted average age calculation. Sample 17NZ124B yielded an error-weighted average $^{206}Pb/^{238}U$ date of 122.0 ± 0.9 (MSWD = 2.2) from seven spots analyzed (Fig. 11F). One much younger date (ca. 110 Ma) was rejected as an outlier.

Puteketeke Pluton

Two granodioritic samples were collected from the Puteketeke Pluton (17NZ98, 17NZ100). Zircons from sample 17NZ100 yielded an error-weighted average $^{206}Pb/^{238}U$ age of 122.6 ± 1.4 Ma (MSWD = 2.7) from nine spots analyzed (Figs. 10 and 11G). Seven zircons from sample 17NZ98 were analyzed and yielded an error-weighted average $^{206}Pb/^{238}U$ age of 122.0 ± 1.6 Ma (MSWD = 0.4; Fig. 11H).

West Arm Leucogranite

The West Arm Leucogranite is a composite unit that consists of orthogneisses (samples 17NZ114 and 17NZ134) and dikes and small plutonic bodies exposed at shore level in Lake Manapouri (samples 17NZ117 and 17NZ137), and larger granitic to granodioritic plutons at higher elevations (samples 17NZ139, 17NZ140, and 17NZ141).

From the orthogneisses, 10 zircons from sample 17NZ114 yielded an error-weighted average $^{206}Pb/^{238}U$ date 123.9 ± 1.5 Ma (MSWD = 1.5; Fig. 11I). Six grains from 17NZ134 yielded a concordant error-weighted average $^{206}Pb/^{238}U$ age of 122.5 ± 1.8 Ma (MSWD = 1.4; Fig. 11J). Three statistically younger grains ranging from 116 to 112 Ma were excluded from the weighted average age calculation.

From the dikes and smaller felsic intrusive bodies, sample 17NZ137 recorded a $^{206}Pb/^{238}U$ age of 113.2 ± 1.3 Ma (MSWD = 3.8) from five zircon spots (Figs. 10 and 11K), with one grain yielding a statistically younger date of ca. 101 Ma. Sample 17NZ117 yielded five concordant dates in five spots with an error-weighted average age of 113.3 ± 1.6 Ma (MSWD = 1.7; Fig. 11L).

From the more massive granodioritic bodies, four of 10 spots analyzed from sample 17NZ139 yielded an error-weighted average $^{206}Pb/^{238}U$ age of 110.3 ± 1.6 Ma (MSWD = 2.3; Fig. 11M). This sample contained a number of xenocrystic zircons with dates of ca. 130–123 Ma, 267 Ma, 320 Ma, and 361 Ma. Sample 17NZ140 yielded an error-weighted average $^{206}Pb/^{238}U$ age of 116.9 ± 1.8 Ma (MSWD = 1.4) from six spots

TABLE 3. SUMMARY OF U-Pb LASER-ABLATION–SPLIT STREAM–INDUCTIVELY COUPLED PLASMA–MASS SPECTROMETRY (LASS-ICP-MS) TITANITE DATES AND ASSOCIATED TEMPERATURES

Sample	P collection no.	Unit*	Rock type	Fabric classification	Titanite type	Date (Ma; 2 SE)	MSWD	No. of titanite†	Temperature§ (°C)	SD (1σ)	Location
17NZ100	P89982	Puteketeke Pluton	bt tonalite	Magmatic (S_0)	Type I	118.4 ± 1.3	0.8	100	694	4	South Arm, Lake Manapouri
17NZ104	P89988	Puteketeke Pluton	bt tonalite	Magmatic (S_0)	Type I	115.7 ± 1.4	1.5	32	697	4	South Arm, Lake Manapouri
17NZ12	P89881	Refrigerator Orthogneiss	hbl-bt tonalite	Low strain (S_1)	Type I	122.3 ± 0.4	7.7	72	700	7	South Fiord, Lake Te Anau
17NZ12	P89881	Refrigerator Orthogneiss	hbl-bt tonalite	Low strain (S_1)	Type I	118.3 ± 0.4	7.7	72	700	7	South Fiord, Lake Te Anau
17NZ11	P89880	Refrigerator Orthogneiss	hbl-bt tonalite	Low strain (S_1)	Type I	121.4 ± 1.5	1.2	28	682	6	South Fiord, Lake Te Anau
17NZ25A	P89896	Refrigerator Orthogneiss	hbl-bt tonalite	Low strain (S_1)	Type I	120.8 ± 1.5	0.8	62	674	7	South Fiord, Lake Te Anau
17NZ124A	P90007	Refrigerator Orthogneiss	bt tonalite	Low strain (S_1)	Type I	117.3 ± 0.8	1.6	48	683	7	West Arm, Lake Manapouri
0213K1	P70481	Indecision Creek shear zone	grt diorite gneiss	Low strain (S_1)	Type II	119.8 ± 2.0	5.9	30	665	5	Steep Hill, Northern Fiordland
0308L1	P70518	Mount Daniel shear zone	bt diorite schist	Low strain (S_1)	Type II	105.5 ± 3.6	1.1	33	689	8	Mount Daniel, Northern Fiordland
0308F	P70512	Mount Daniel shear zone	grt diorite gneiss	High strain (S_2)	Type II	111.1 ± 1.2	0.7	42	631	7	Mount Daniel, Northern Fiordland
17NZ4A	P89869	Lake Hankinson Complex	bt gneiss	High strain (S_2)	Type II	125.3 ± 1.4	4.2	40	690	5	South Fiord, Lake Te Anau
17NZ31A	P89897	Murchison intrusives	hbl diorite mylonite	High strain (S_2)	Type II	125.7 ± 7.4	0.6	37	620	6	South Fiord, Lake Te Anau
17NZ43A	P89913	Murchison intrusives	diorite mylonite	High strain (S_2)	Type II	123.2 ± 9.6	0.4	21	608	6	South Fiord, Lake Te Anau
17NZ55A	P89930	Hunter intrusives	hbl-bt tonalite mylonite	High strain (S_2)	Type II	146.8 ± 2.3	2.4	34	637	4	South Fiord, Lake Te Anau
17NZ60	P89934	Hunter intrusives	hbl diorite mylonite	High strain (S_2)	Type II	116.3 ± 1.7	0.4	28	659	7	South Fiord, Lake Te Anau
17NZ72A	P89950	Hunter intrusives	hbl diorite protomylonite	High strain (S_2)	Type II	130.8 ± 1.8	1.1	66	650	7	South Fiord, Lake Te Anau
17NZ95B	P89975	Lake Manapouri mylonite	hbl-bt diorite mylonite	High strain (S_2)	Type II	117.1 ± 3.2	2.3	40	699	7	South Arm, Lake Manapouri
17NZ95B	P89975	Lake Manapouri mylonite	hbl-bt diorite mylonite	High strain (S_2)	Type II	307.7 ± 3.7	28.0	28	699	7	South Arm, Lake Manapouri
17NZ96	P89978	Lake Manapouri mylonite	bt diorite mylonite	High strain (S_2)	Type II	122.3 ± 1.8	2.3	18	658	**7**	South Arm, Lake Manapouri

Note: Mineral abbreviations are after Whitney and Evans (2010): bt—biotite; grt—garnet; hbl—hornblende. MSWD—mean square of weighted deviates; SE—standard error; SD—standard deviation.
*Unit names follow Turnbull et al. (2010).
†Titanite grains used in age calculations.
§Titanite temperatures calculated from Ti concentrations following Hayden et al. (2008) thermometer.

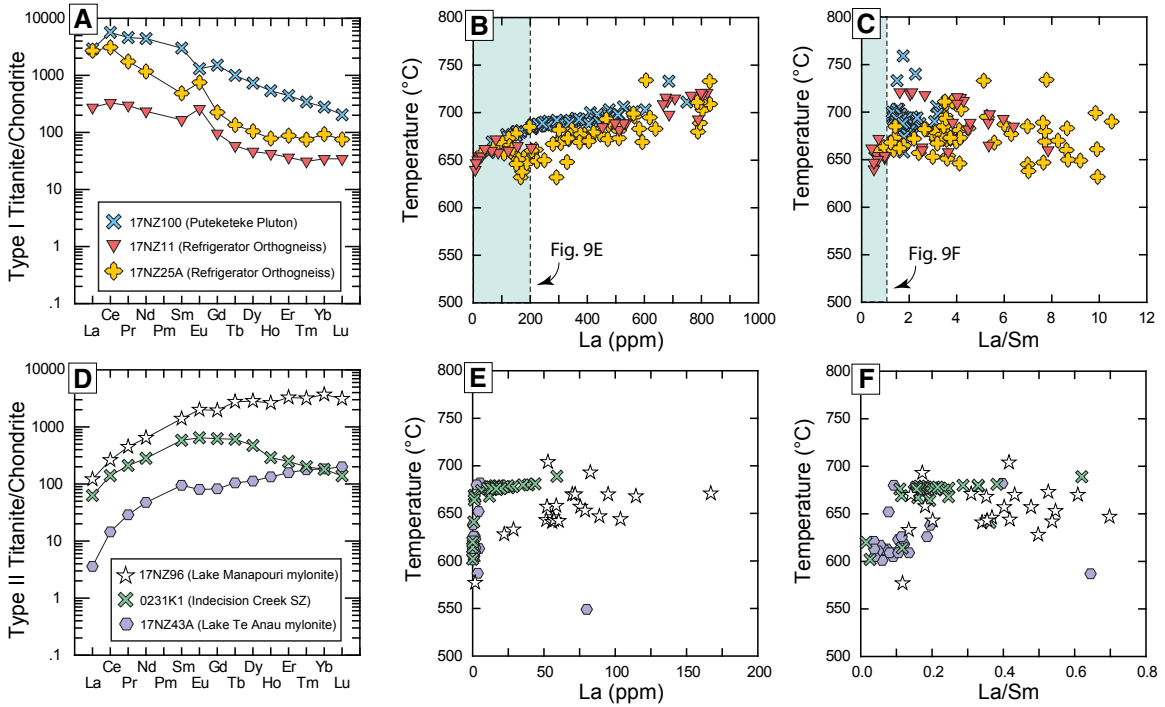

Figure 9. (A) Chondrite-normalized rare earth element abundance patterns for representative type I titanites. (B) Temperature vs. La (ppm) for representative type I titanites. (C) Temperature vs. La/Sm for representative type I titanites. (D) Chondrite-normalized rare earth element abundance patterns for representative type II titanites. (E) Temperature vs. La (ppm) for representative type II titanites. (F) Temperature vs. La/Sm for representative type II titanites. SZ—shear zone.

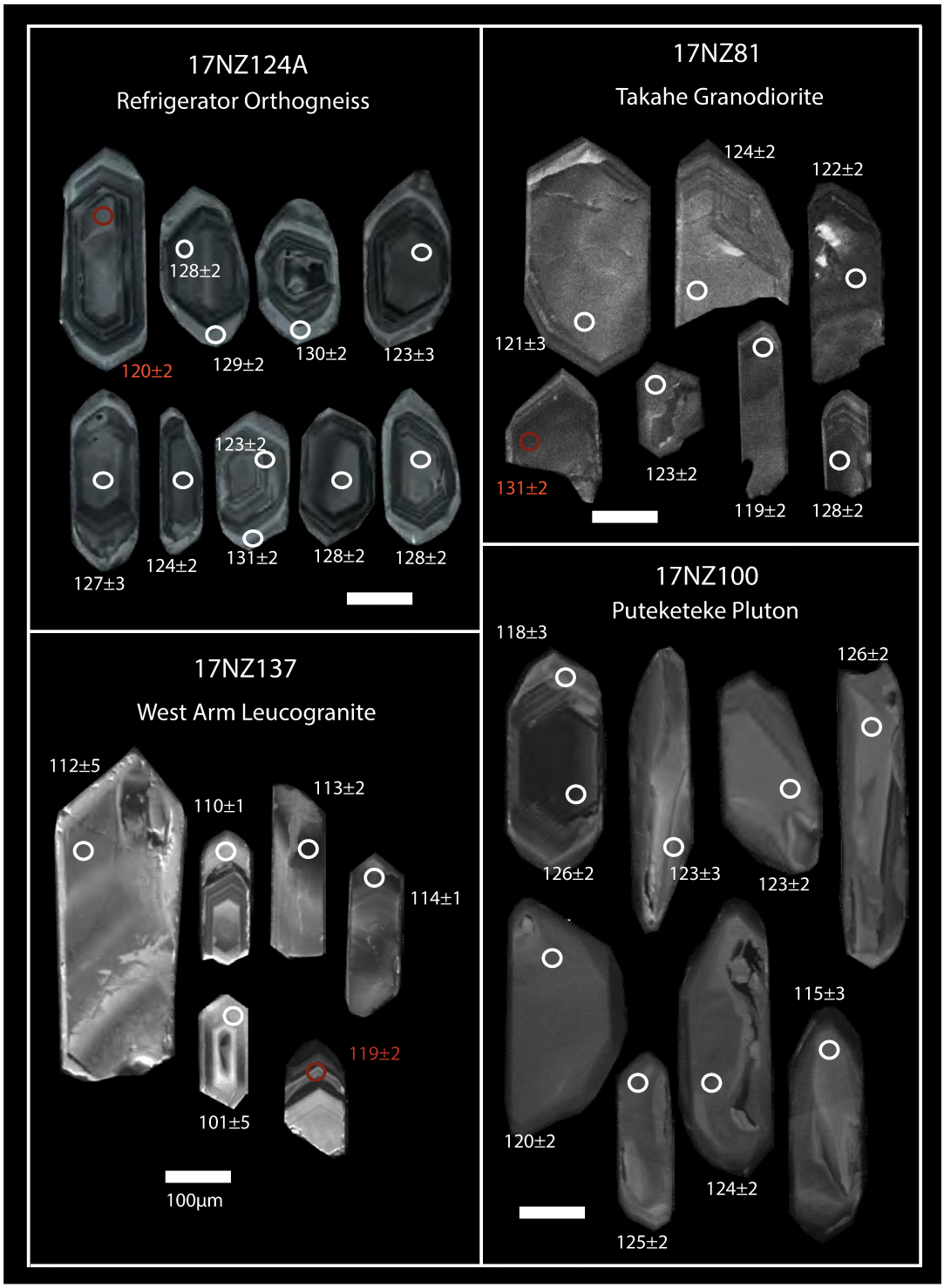

Figure 10. Representative cathodoluminescence (CL) images for Separation Point Suite and Carboniferous and Darran Suite samples. White circles (~30 µm in diameter) show spots targeted during the sensitive high-resolution mass spectrometer–reverse geometry (SHRIMP-RG) analyses. Red spots show analyses excluded from error-weighted average age calculation. Scale bars are 100 µm. Age uncertainty is 1σ. (***Continued on following page.***)

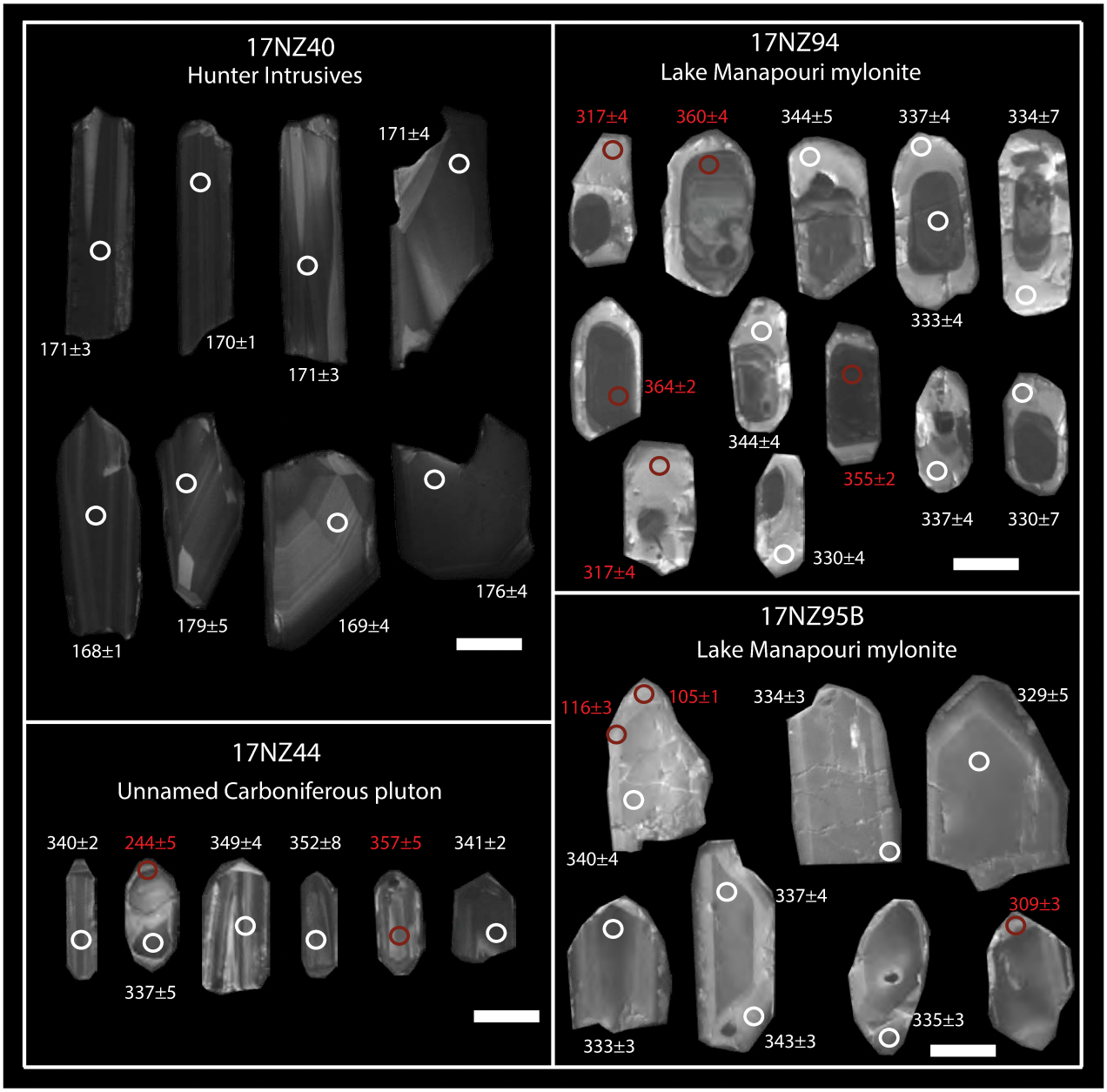

Figure 10 (*continued*).

(Fig. 11N), and it also had older zircons with dates of ca. 330 and 497 Ma. Nine grains from sample 17NZ141 yielded a concordant error-weighted average $^{206}Pb/^{238}U$ age of 118.0 ± 1.1 Ma (MSWD = 2.7; Fig. 11O). One older grain gave a date of 220 Ma.

Takahe Granodiorite

Two tonalites were collected from within the Takahe Granodiorite (17NZ78B, 17NZ81). Six zircon grains from sample 17NZ81 gave an error-weighted average $^{206}Pb/^{238}U$ age of 123.2 ± 1.8 Ma (MSWD = 1.9; Figs. 10 and 11P). One older grain with a date of 131 Ma was excluded from the weighted average age calculation. For sample 17NZ78B, nine analyses yielded an error-weighted average $^{206}Pb/^{238}U$ age of 125.2 ± 1.6 Ma (MSWD = 0.3; Fig. 11Q).

Carboniferous and Darran Suite

Lake Manapouri Mylonites

Two samples, 17NZ94 and17NZ95B, were analyzed from mylonites on South Arm, Lake Manapouri. Zircons from 17NZ94 yielded an error-weighted average $^{206}Pb/^{238}U$ age of 336.3 ± 3.2 Ma for a population of luminescent rims and cores (MSWD = 1.6; n = 6; Figs. 10 and 11R). Rims had Th/U values ranging from 0.5 to 0.7 and overgrew dark cores that had distinctly higher Th and U concentrations compared to the ca. 336 Ma population. These dark cores ranged in age from 355 to 364 Ma, and we interpret them as xenocrysts (Fig. 10). Two other spots were younger (ca. 317 Ma) and likely represent Pb loss. Seven spots analyzed from rims and interior domains on sample 17NZ95B yielded an error-weighted average

TABLE 4. SUMMARY OF U-Pb SENSITIVE HIGH-RESOLUTION MASS SPECTROMETER–REVERSE GEOMETRY (SHRIMP-RG) ZIRCON DATES AND ASSOCIATED TEMPERATURES

Sample	P collection no.	Latitude (°S)	Longitude (°E)	Unit*	Rock type	Date (Ma; 2 SE)	MSWD	No. of zircons†	Temperature§ (°C)	SD (1σ)
17NZ12	P89881	45.293	167.481	Refrigerator Orthogneiss	hbl-bt tonalite	128.8 ± 1.7	2.8	10	800	8
17NZ25A	P89896	45.309	167.475	Refrigerator Orthogneiss	hbl-bt tonalite	129.2 ± 1.7	0.8	8	827	8
17NZ25B	P89896	45.309	167.475	Refrigerator Orthogneiss	postkinematic pegmatite dike	124.1 ± 1.4	2.8	7	801	8
17NZ40	P89906	45.309	167.522	Murchison intrusives	diorite mylonite	170.0 ± 1.5	1.2	8	870	9
17NZ43B	P89914	45.307	167.520	Murchison intrusives	postkinematic pegmatite dike	344.5 ± 1.8	5.2	7	727	7
17NZ44	P89915	45.313	167.526	Hunter intrusives	granite	342.8 ± 2.5	3.2	6	649	7
17NZ78B	P89960	45.341	167.649	Takahe Granodiorite	bt granodiorite	125.1 ± 1.7	0.3	9	609	6
17NZ81	P89963	45.340	167.669	Takahe Granodiorite	bt granodiorite	123.2 ± 1.8	1.9	6	627	6
17NZ94	P89973	45.553	167.417	Lake Manapouri mylonite	bt-hbl diorite mylonite	336.3 ± 3.2	1.6	6	817	8
17NZ95B	P89975	45.555	167.415	Lake Manapouri mylonite	hbl-bt diorite mylonite	336.2 ± 2.4	1.7	7	712	7
17NZ98	P89980	45.552	167.400	Puteketeke Pluton	bt granodiorite	122.0 ± 1.6	0.4	7	626	6
17NZ100	P89982	45.547	167.402	Puteketeke Pluton	bt tonalite	122.6 ± 1.4	2.7	9	593	6
17NZ114	P89998	45.507	167.349	West Arm Leucogranite	hbl-bt tonalite	123.9 ± 1.5	1.5	10	828	9
17NZ117	P90001	45.509	167.344	West Arm Leucogranite	bt granodiorite	113.3 ± 1.6	1.7	5	606	6
17NZ124A	P90007	45.494	167.397	Refrigerator Orthogneiss	bt tonalite	127.4 ± 1.3	2.0	10	672	7
17NZ124B	P90008	45.494	167.397	Refrigerator Orthogneiss	postkinematic pegmatite dike	122.0 ± 0.9	2.2	6	653	7
17NZ127	P90010	45.493	167.385	Refrigerator Orthogneiss	postkinematic pegmatite dike	112.7 ± 1.3	1.2	8	590	6
17NZ134	P90013	45.449	167.374	West Arm Leucogranite	hbl-bt tonalite	122.5 ± 1.8	1.4	6	785	8
17NZ137	P90016	45.491	167.355	West Arm Leucogranite	bt tonalite	113.2 ± 1.3	3.8	5	646	6
17NZ139	P90018	45.565	167.313	West Arm Leucogranite	bt granite	110.3 ± 1.6	2.3	4	712	7
17NZ140	P90019	45.550	167.312	West Arm Leucogranite	bt granodiorite	116.9 ± 1.8	1.4	6	699	7
17NZ141	P90020	45.532	167.275	West Arm Leucogranite	bt granodiorite	118.0 ± 1.1	2.7	9	710	7

Note: Complete isotopic data and individual spot dates can be found in the supplementary file (see text footnote 1). Mineral abbreviations are after Whitney and Evans (2010): bt—biotite; hbl—hornblende. MSWD—mean square of weighted deviates; SE—standard error; SD—standard deviation

*Unit names follow Turnbull et al. (2010).

†Zircons used in age calculations.

§Zircon temperatures calculated from Ti concentrations following Watson et al. (2006) thermometer.

$^{206}Pb/^{238}U$ age of 336.3 ± 2.4 Ma (MSWD = 1.7; Figs. 10 and 11S), with three grains yielding statistically younger dates of 105 Ma, 116 Ma, and 309 Ma. The two Cretaceous dates were analyzed on a thin (<20 µm thick) rim, and the oldest date is similar to the lower-intercept age of titanites from the same sample (117.1 ± 3.2 Ma; see above).

Murchison and Hunter Intrusives (Darran Suite)

Zircon grains from four samples (17NZ40, 17NZ43A, 17NZ43B, 17NZ44) mapped as Darran Suite exhibited subhedral to anhedral crystal shape and homogeneous zoning, with occasional subordinate sector and patchy zonation. Samples 17NZ43A and 17NZ43B mapped as Murchison intrusives by Turnbull et al. (2010) and Allibone et al. (2009a) gave Carboniferous dates. Seven spots from sample 17NZ43B yielded a population with a $^{206}Pb/^{238}U$ age of 344.5 ± 1.8 Ma (MSWD = 5.2; Fig. 11T). This sample also contained two statistically older grains ranging in age from 367 to 359 Ma, and one younger grain at 314 Ma. The host rocks gave an LA-SF-ICP-MS (SF—sector field) zircon age of 344.0 ± 7.6 Ma (17NZ43A: M. Ringwood, 2018, personal commun.), which overlaps with our age for the postkinematic felsic dike. Sample 17NZ44, mapped as Hunter intrusive in Turnbull et al. (2010) and Allibone et al. (2009a), yielded an error-weighted average $^{206}Pb/^{238}U$ age of 342.8 ± 2.5 Ma (MSWD = 3.2) from six spot analyses (Figs. 10 and 11U). Eight spots from sample 17NZ40 (Murchison intrusive) yielded an error-weighted average $^{206}Pb/^{238}U$ age of 170.0 ± 1.5 Ma (MSWD = 1.2; Figs. 10 and 11V).

DISCUSSION

Linking Titanite Petrochronology and Transpressional Shear Zone Development

Our field and petrographic investigation of magmatic and deformational structures in Lake Te Anau and Lake Manapouri revealed a pattern of magmatism and deformation that was synchronous with the development of distinct titanite morphologies and chemistries in magmatic and deformed rocks. These features provide insights into the timing and temperature conditions of deformation in the middle and lower crust of the Median Batholith during a major Cordilleran arc flare-up event (Milan et al., 2017; Schwartz et al., 2017). From our field mapping, we observed the following key features that guided our interpretations: (1) Igneous structures and textures (S_0) are primarily preserved in undeformed Separation Point Suite plutons such as the Puteketeke Pluton (123–122 Ma), the West Arm Leucogranite (124–111 Ma), and the Takahe Granodiorite (125–123 Ma); (2) low-strain fabrics overprint magmatic structures and record shallowly dipping foliations (S_1) and shallowly plunging lineations (L_1), and such structures are generally associated with euhedral, type I titanites; and (3) high-strain zones overprint all other structures and contain amphibolite-facies mineral assemblages, moderately to steeply dipping foliations (S_2), and moderately to steeply plunging lineations (L_2). These fabrics are associated with anhedral titanite grains and aggregates that we classify as type II titanites. Next, we link these field observations with microscale geochemical and isotopic observations from titanites to understand the timing and thermal conditions of transpressional deformation during arc construction.

Early, Low-Strain (S_1) Fabric Development

In the middle crust of central Fiordland, shallowly to moderately dipping low-strain fabrics occur within the Darran Suite and the Refrigerator Orthogneiss of the Separation Point Suite (Fig. 2B). In Lake Manapouri, we observed these fabrics primarily in the Refrigerator Orthogneiss; however, to the north in Lake Te Anau, low-strain domains occur over a broader zone, up to 15 km wide. In this region, low-strain domains form the western boundary of a broad zone that is cored by a number of high-strain, subvertical mylonitic shear zones (see below). Based on crosscutting relationships, low-strain fabrics appear to predate high-strain

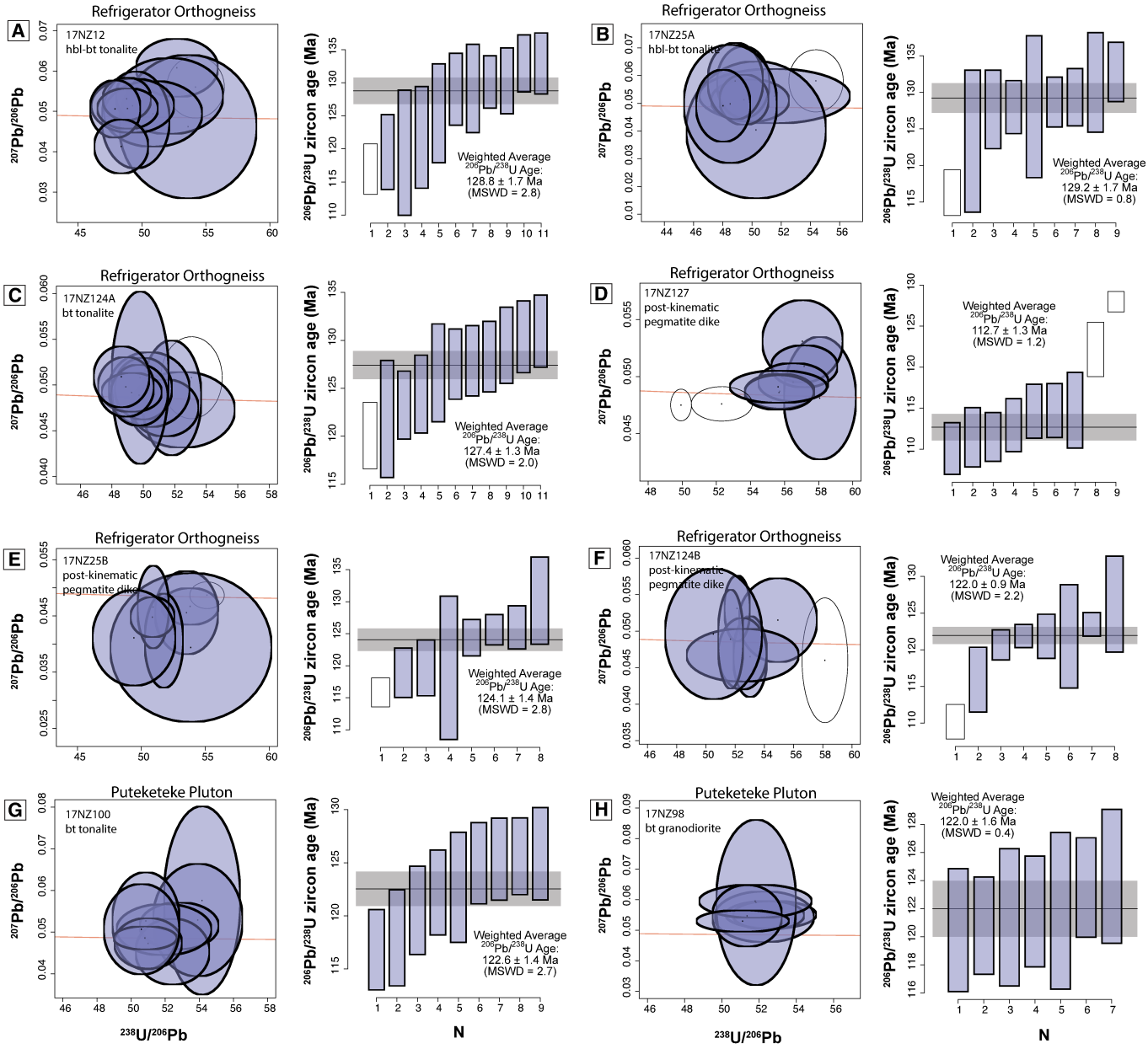

Figure 11. Tera-Wasserburg concordia diagrams and weighted average age plots (wtd—weighted; conf—confidence; rej—rejected) for zircon data. Concordia and weighted average diagrams show all spots (including rejected spots in white). Error ellipses show 2σ total uncertainty for spot analyses. MSWD—mean square of weighted deviates; bt—biotite; hbl—hornblende. (*Continued on following page.*)

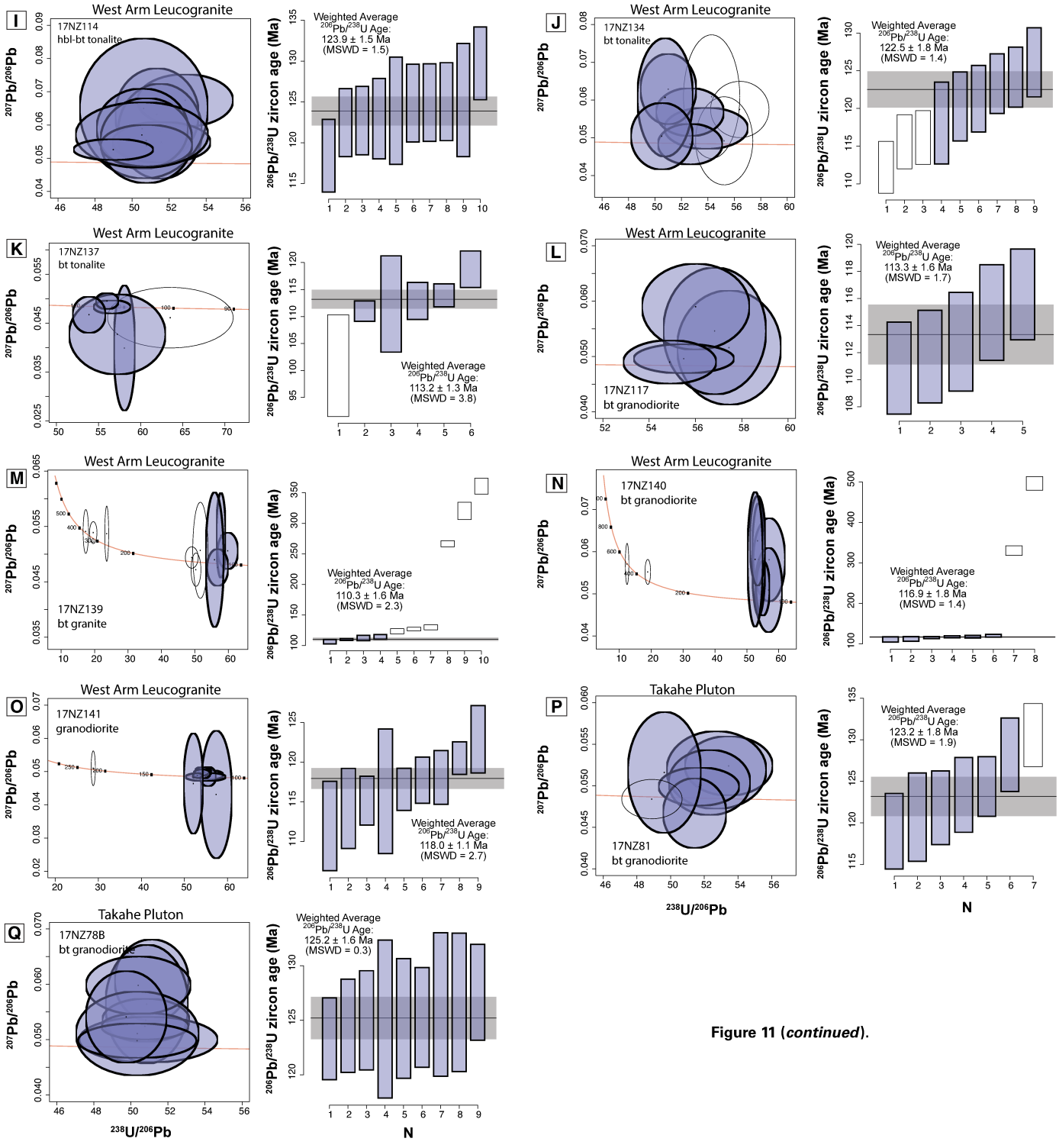

Figure 11 (*continued*).

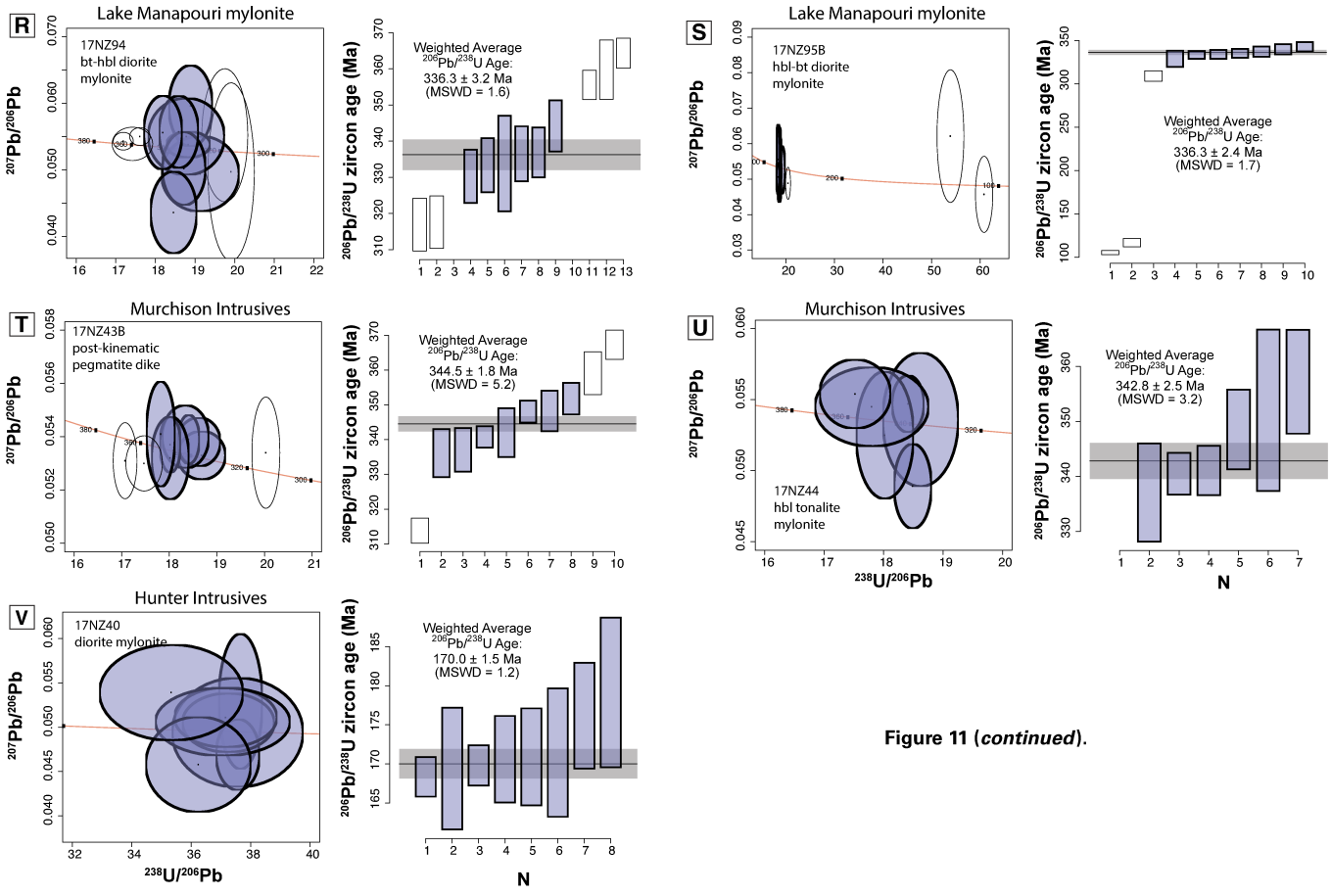

Figure 11 (*continued*).

mylonitic fabrics, which contain amphibolite-facies mineral assemblages and formed at midcrustal conditions (Scott et al., 2009).

The timing of low-strain fabric formation is best constrained by observations from the Refrigerator Orthogneiss. Regional structural mapping shows that it contains distinct structural fabrics consisting of shallow to moderate foliations striking 019°–085° and dipping 28°–54° southeast, and south-trending lineations with shallow plunges (12°–40°). Zircons from host rocks that contain these fabrics give error-weighted average $^{206}Pb/^{238}U$ crystallization ages ranging from 129.1 ± 1.8 Ma to 127.4 ± 2.0 Ma. Postkinematic dikes that crosscut low-strain fabrics range from 124.9 ± 2.7 Ma to 112.7 ± 1.8 Ma. These data indicate that low-strain fabric development in the middle crust is bracketed between ca. 127.4 and 124.9 Ma, which overlapped with the initiation of the Separation Point Suite flare-up event in the Median Batholith.

Titanites from low-strain fabrics are millimeter-size euhedral wedges and show no evidence for postmagmatic recrystallization or metamorphic growth in thin section or BSE images (Figs. 4 and 6). They are characterized by LREE/HREE enrichment and broad intrasample crystallization temperatures that range up to ~150 °C (see summary of type I titanites in Fig. 12). Rock-average Zr-in-titanite temperatures range from 675 °C to 700 CC, although individual grains record temperatures up to ~750 °C (Data Repository Item). Hornblende-plagioclase thermometry give similar equilibration temperatures ranging from 676 °C to 695 °C (Scott et al., 2009). We follow other works in interpreting these textural and geochemical features as magmatic in origin (Smith et al., 2009; Kohn and Corrie, 2011; Gao et al., 2012; Cao et al., 2015; Fu et al., 2016; Garber et al., 2017). Lower-intercept ages range from 122.3 Ma to 117.3 Ma, which overlap with and are also younger than low-strain fabric formation bracketed by zircon ages from host and postkinematic dikes (ca. 127.4–124.9 Ma). Therefore, these titanites are most consistent with igneous growth during magmatic cooling, and their dates likely reflect cooling though the titanite closure temperature of ~650 °C (rather than subsolidus growth during S_1 flow).

High-Strain Fabric Development

High-strain shear zones are recognized throughout Fiordland and Stewart Island in the middle and lower crust (e.g., Allibone and Tulloch, 2008; Klepeis et al., 2004, 2007; Marcotte et al., 2005). In northern Fiordland, high-strain fabrics are present in parts of the Indecision Creek shear zone (Marcotte et al., 2005) and the Mount Daniel shear zone (Klepeis et al., 2004); in central Fiordland, they occur in Lake Manapouri (and southward to Lake Hauroko), and in a number of diffuse and narrow shear zones in South Fiord, Lake Te Anau (Figs. 2A–2B).

The high-strain zone in Lake Manapouri is the largest of the midcrustal, Early Cretaceous high-strain zones and is characterized by a 200–300-m-wide zone of north-striking L-S tectonites (e.g., Scott et al., 2009, 2011; Scott, 2013). Structural measurements and variations in finite strain (i.e., fabric intensity, percentage matrix-porphyroclasts) suggest that the boundaries of this zone are vertical/subvertical and parallel the overall trend of the arc. Our mapping in Lake Te Anau and Lake Manapouri shows that these high-strain zones are part of a complex 20-km-wide zone of mylonitic deformation. We refer to this broad zone of mid-crustal

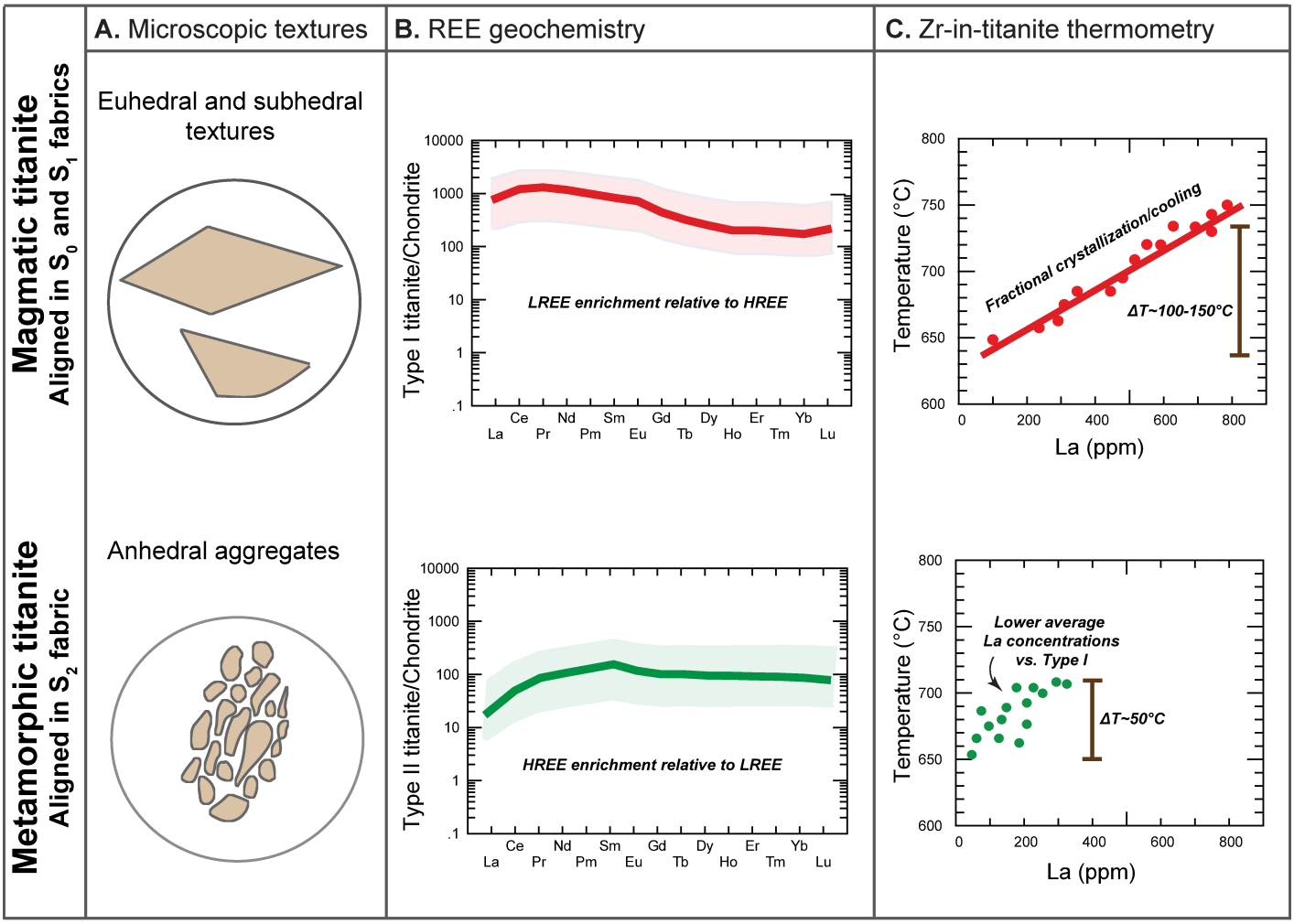

Figure 12. Summary of titanite classification based on: (A) textural relations; (B) chondrite-normalized rare earth element (REE) patterns (LREE—light REEs, HREE—heavy REEs); and (C) binary plots of temperature vs. trace-element compositional variation of lanthanum (La).

deformation as the Grebe shear zone, which includes both the early low-strain fabrics described above and the higher-strain mylonitic zones (e.g., Lake Manapouri and Lake Te Anau mylonites). Shear-zone fabrics in this zone are characterized by lineations with shallow plunges (~20°–40°) in low-strain zones and moderate to steep plunges (60°–90°) in high-strain zones. Our observations do not allow us to evaluate whether the observed steepening of lineations represents progressively accumulated strain or two superimposed events. However, low-strain fabrics are generally older (129–125 Ma) compared to high-strain fabrics (126–116 Ma), suggesting that the two fabrics are either genetically unrelated and/or represent pulses of transpressional deformation that were separated in time.

In Lake Manapouri, interpretation of deflected quartz ribbons and asymmetric plagioclase porphyroclasts in the motion plane (normal to foliation, parallel to lineation) of mylonitic rocks indicates an overall sinistral strike-slip component of displacement parallel to the trend of the Median Batholith (Scott et al., 2011; Hufford, 2018; McGinn, 2018). An apparently normal-sense (west-side-down) component of motion is also suggested by the moderate SW plunge of lineations within the steeply west-dipping foliation of the Lake Manapouri mylonites. The sinistral strike-slip and normal-sense components of motion, when combined with gently plunging crystallographic vorticity axes of these mylonites (Hufford, 2018; McGinn, 2018), are consistent with inclined transpression. In inclined transpression, one of the shear zone boundaries is defined by a normal fault or shear zone, with the other boundary having a thrust component as a result of the non-coaxiality of both strike-slip and dip-slip components of strain. In this way, the apparently normal-sense motion along the steeply west-dipping Lake Manapouri mylonites is interpreted as a consequence of inclined transpression (e.g., Jones et al., 2004), which precludes the need to invoke rotation to explain its current geometry (Scott et al., 2011).

In this interpretation, the 20-km-wide zone of transpressional deformation in the Grebe shear zone consists of a western boundary (e.g., Lake Manapouri mylonites) with oblique normal-sense motion and an eastern boundary with thrust-sense motion (predicted but not observed in this study). This model of inclined transpression implies uplift of the outboard Median Batholith relative to the inboard Batholith (i.e., east-side-up motion), which is consistent with amphibole and biotite ^{40}Ar-^{39}Ar thermochronology from the Lake Manapouri area. For example, Scott et al. (2011) reported ^{40}Ar-^{39}Ar amphibole (127.9–123.7 Ma) and biotite (122.1–117.3 Ma) dates east of the Grebe shear zone that are consistently older than amphibole (112.7–111.4 Ma) and biotite (101.8 Ma) dates to the west. Inclined transpressional features are also consistent with the deformation geometry in the Indecision Creek shear zone, and both can

be linked as a network of middle- to lower-crustal triclinic, transpressional shear zones (Marcotte et al., 2005; Klepeis and King, 2009).

Transpressional structures in Lake Manapouri are spatially associated with the development of broad (kilometer-scale), synmagmatic, open folds, with minor, outcrop-scale S and Z folds in the limbs of the open fold west of the shear zone in the Puteketeke Pluton (Fig. 3B). The Z folding is characterized by top-to-the-SW vergence with fold limbs striking from 041° to 045° and dipping from 32° to 68° SE. In some places, the Puteketeke Pluton also crosscuts high-strain fabrics in the Grebe shear zone (R. Jongens, 2018, personal commun.), indicating that mylonitic shearing and Puteketeke Pluton emplacement temporally overlapped (Fig. 3C).

Hypersolidus folding adjacent to the Grebe shear zone suggests that some strain was accommodated by late deformation in the Puteketeke Pluton; however, quantification of the absolute magnitude of strain accommodated is inherently difficult because magmatic fabrics rarely, if ever, preserve their entire strain history, and hypersolidus foliations and folds only preserve the last increment of strain during crystallization (Paterson et al., 1998; Webber et al., 2015; Fossen and Calvacante, 2017). In the case of the Puteketeke Pluton, its high Sr/Y chemistry and depletion in HREEs suggest that it was derived in part from partial melting of mafic arc crust in the garnet-stability field at depths greater than or equal to ~35 km at 122.8–119.9 Ma (Tulloch and Kimbrough, 2003; Scott and Palin, 2008; Allibone et al., 2009b; Ramezani and Tulloch, 2009; this study). The emplacement depth of the Puteketeke Pluton at ~20–24 km depth (Scott et al., 2009) would have allowed vertical displacements of at least 11–15 km or more prior to emplacement in the middle crust. Unfolding of hypersolidus fabrics also provides an estimate for horizontal shortening during the last increment of deformation. Based on foliation measurements from the south shore of Lake Manapouri, we estimate ~2%–3% of horizontal shortening for this final increment of the deformation. We emphasize that this is a minimum estimate for the magnitude of horizontal shortening, because the majority of strain is not preserved in the pluton.

In contrast to hypersolidus fabrics, mylonitic fabrics preserve more information on the magnitude of displacement accommodated during midcrustal transpression. Using the length-displacement relationship of Pennacchioni (2005), we estimate ~10 km of offset, given the length of the Grebe shear zone. Foliation deflection trajectories in the Lake Manapouri area are also consistent with several kilometers of strike-slip displacement (Ramsay and Huber, 1983). Both independent measurements together suggest as much as 10 km of lateral offset during the mylonitic phase of shearing at ca. 122–117 Ma. Quantifying vertical displacements along the Grebe shear zone is more difficult because there is little pressure information directly correlated with mylonitic deformation. Pressure information from Jurassic to Cretaceous plutonic rocks on either side of the Grebe shear zone give an average of 3 km of west-side-up vertical displacement (Scott et al., 2009). However, the timing of this uplift is uncertain, and the west-side-up sense of shear contrasts with thermochronologic data that indicate the opposite sense of motion (west-side-down). One problem with use of the barometric data is that pressure estimates east and west of the fault are derived from rocks of contrasting ages (Jurassic-age rocks east, Cretaceous-age rocks west), and they assume no subsequent reactivation of the fault. Geologic mapping of the region shows a possible Tertiary brittle structure that parallels the Grebe shear zone in South Arm, Lake Manapouri (Turnbull et al., 2010), and we cannot rule out that Tertiary movement and/or reactivation of this fault may have resulted in the observed pressure difference along the Grebe shear zone (Klepeis et al., 2019). Therefore, we are cautious about assigning specific vertical displacements to the Grebe shear zone in the Early Cretaceous.

Titanites from the high-strain portions of the Grebe shear zone provide additional insights into the temperature conditions of deformation during fabric development. Type II titanites in these rocks are characterized by anhedral grains or aggregates of anhedral grains that are aligned within mylonitic fabrics (Fig. 5). In chondrite-normalized rare earth element (REE) plots, titanites display HREE depletion relative to LREE, and low La concentrations relative to type I, igneous titanites (see summary of type I and II titanites in Figs. 9 and 12). Middle (M) REEs are more strongly partitioned into type II titanites than LREEs, and this behavior has been associated with metamorphic reactions in several titanite geochemical studies (Della Ventura et al., 1999; Olin and Wolff, 2012; Che et al., 2013; Garber et al., 2017; Loader et al., 2017). Zr-in-titanite temperatures generally show a narrow crystallization range (typically <50 °C), and rock-average temperatures range from ~610 °C to 700 °C, with the highest temperature recorded in the Lake Manapouri mylonites (660–700 °C) and slightly lower average temperatures recorded in the Lake Te Anau mylonites (610–660 °C). We note that our titanite temperatures are consistently higher than deformation temperatures reported by Scott et al. (2011). They reported rock-average garnet-biotite temperatures of 576 ± 53 °C and 588 ± 58 °C (assuming pressures of 3 and 10 kbar); however, their temperatures were not linked to dates and may record an earlier phase of metamorphism, such as that observed in titanites from the Lake Manapouri mylonites in this study (samples 17NZ95b and 17NZ96 in Figs. 8G–8H).

Titanites in the Lake Te Anau mylonites generally give Cretaceous lower-intercept dates ranging from 125.7 to 116.3 Ma, and titanites from the Lake Manapouri mylonites give overlapping lower-intercept dates ranging from 122.3 to 117.1 Ma. Scott et al. (2009) reported a similar titanite date of 119.6 ± 4.7 Ma from a mylonitized pluton south of South Arm, Lake Manapouri, and ^{40}Ar-^{39}Ar biotite dates from eastern Lake Manapouri suggest cooling of the outboard Median Batholith through ~325 °C between 122.1 and 117.3 Ma (Scott et al., 2011). These dates and our dates overlap with the timing of igneous crystallization and hypersolidus folding observed in the adjacent Puteketeke Pluton (122.8–119.9 Ma: Scott and Palin, 2008; Ramezani and Tulloch, 2009; this study), suggesting that deformation was synchronous with mid-crustal magmatism.

Pre-Cretaceous titanites were also observed in the Lake Manapouri mylonites and yielded poorly constrained lower-intercept dates of ca. 307 Ma (Figs. 7G–7H). These older dates may be related to medium-pressure–high-temperature metamorphism in central Fiordland at 340–315 Ma (Ireland and Gibson, 1998; Flowers et al., 2005; Chavez et al., 2007; Daczko et al., 2009; Schwartz et al., 2016; Dwight et al., 2018) and may signify incomplete purging of older titanite domains during Cretaceous mylonitic deformation at amphibolite-facies conditions. Thus, titanite textures and variations in dates indicate preservation of complex growth and (re)crystallization, and ^{206}Pb/^{238}U dates cannot be attributed to thermally activated volume-diffusion or simple core-rim crystallization processes (see 17NZ95B in Fig. 7). Instead, our observations of type II titanites are most consistent with titanite dates recording (re)crystallization in response to deformation and/or metamorphic reactions during amphibolite-facies metamorphism.

Further to the north in the lower crust, two samples from the Mount Daniel shear zone (domain i of Marcotte et al., 2005) yielded titanite dates ranging from 111.1 Ma (0308F) to 105.5 Ma (0308L1). Both samples gave Zr-in-titanite temperatures ranging from 630 °C to 690 °C and signify a period of high- to moderate-strain, amphibolite-facies deformation from ca. 111 to 106 Ma. Outcrop textures for these sample show that early granulite-facies shearing occurred synchronously with emplacement of the Worsley Pluton (124.0–121.8 Ma; Schwartz et al., 2017, and references therein), and our dates suggest that the latest motion of the Mount Daniel shear zone lasted until 111–106 Ma. These dates overlap with the timing of extensional structures further south in western Fiordland (Klepeis et

al., 2016; Schwartz et al., 2016); however, we did not observe evidence for extensional structures in northern Fiordland.

Along the western margin of the Indecision Creek shear zone, sample 0213K1 from the early, S_1 high-grade fabric yielded a lower-intercept date of 119.8 Ma ± 2.0 Ma and an average Zr-in-titanite temperature of ~670 °C, consistent with amphibolite-facies deformation. Marcotte et al. (2005) reported a zircon rim date of 119.0 ± 4.7 Ma from a late-stage dike that cuts the earlier S_1 and S_2 fabrics at this location. Our date and theirs establish that the timing of S_1 and S_2 formation occurred at ca. 120–119 Ma. Higher-strain, transpressional fabrics located in the core of the Indecision Creek shear zone (domain iii in Fig. 2A) formed slightly later at 115.0 ± 3.6 Ma (Marcotte et al., 2005), which temporally overlaps with the development of high-strain, transpressional fabrics in the middle crust of central Fiordland. Collectively, these data show that transpressional fabrics in both the middle and lower crust coincided with a major pulse of mafic to felsic magmatism during the arc flare-up event, and transpression in both levels of the crust preceded the onset of extensional orogenic collapse of the Median Batholith at ca. 108–106 Ma (Klepeis et al., 2016; Schwartz et al., 2016).

Two mylonitic samples (17NZ55 and 17NZ72A) from Lake Te Anau also record older lower-intercept dates ranging from 146.8 to 130.7 Ma (Figs. 6 and 7M–7N). The latter date overlaps with the timing of the low-strain fabrics we observed in the Refrigerator Orthogneiss and may indicate that both low- and high-strain fabrics developed synchronously during the initiation of the Separation Point Suite flare-up event. In contrast, the ca. 147 Ma date is older than the other high-strain fabrics that we observed in central and northern Fiordland and may signal an older, unrecognized phase of arc-parallel deformation and metamorphism within the Median Batholith. Evidence for a late Tithonian event may also be preserved in garnet-bearing pelitic gneisses in central Fiordland. Scott et al. (2009) reported a metamorphic zircon date of 145.0 ± 2.8 Ma, and pressure-temperature data indicate that zircon growth and metamorphism occurred at amphibolite-facies conditions (4.2 ± 0.8 kbar and 629 ± 20 °C). Further research is needed in the Darran Suite and older arc rocks to better constrain this event(s).

Spatial and Temporal Patterns of Arc Magmatism and Deformation in Central Fiordland

We compiled our geochronological and structural results along with results from previous geochronology studies to document the temporal evolution of magmatism and deformation in the middle and lower crust of Fiordland. These data are summarized in Figures 13 and 14. Our compilation reveals that plutonism in the Fiordland sector of the Median Batholith consisted of three primary episodes: a high-magma-addition-rate pulse of S-, I-, and A-type plutons in the Devonian from ca. 365 to 345 Ma, followed by low-magma-addition-rate plutonism until ca. 305 Ma (Tulloch et al., 2009; Turnbull et al., 2016), a prolonged period of low-magma-addition-rate magmatism from ca. 240 to 130 Ma (Darran Suite; Kimbrough et al., 1994; Allibone et al., 2009b; Milan et al., 2016, 2017; Schwartz et al., 2017), and a terminal high-magma-addition-rate event from 129 to 110 Ma (see Figs. 14A–14E for Mesozoic magmatic pulses). This terminal phase involved the emplacement of granitic to tonalitic melts of the Separation Point Suite magmatism in the shallow to middle crust of central Fiordland, and gabbros and diorites in the lower crust in western Fiordland (Western Fiordland Orthogneiss). While several previous studies have documented the tempo of magmatism in the lower crust (Schwartz et al., 2017, and references therein), prior to this study, large portions of the middle crust in Fiordland remained poorly dated, and their temporal relationships to deformation remained unclear.

Our 22 new SHRIMP-RG zircon ages from central Fiordland provide new insights into this problem and link low- and high-strain fabric development to plutonism in the middle and lower crust. We find that middle-crustal deformation was closely associated temporally and spatially with emplacement and crystallization of the Separation Point Suite. This surge of midcrustal magmatism in central Fiordland involved punctuated emplacement of plutons over ~19 m.y. from 129 to 110 Ma. The initiation of the high-magma-addition-rate event involved early dioritic to tonalitic plutonism in the Refrigerator Orthogneiss (129–127 Ma). This early phase of Separation Point Suite magmatism is rare in the Median Batholith (Fig. 14B) and signifies an important change in magma chemistry from dominantly low-Sr/Y plutonism that characterizes the Darran Suite to strongly high-Sr/Y plutonism that characterizes the Separation Point Suite. Small volumes of similar-age plutons appear in the lower crust (e.g., Supper Cove Pluton, and Mount Edgar Diorite; Hollis et al., 2003; Tulloch and Kimbrough, 2003) and in upper-crustal exposures in southwest Fiordland (e.g., Rahu Suite; Gollan et al., 2005; Ramezani and Tulloch, 2009). The Refrigerator Orthogneiss is significant in that it is the earliest phase of Separation Point Suite magmatism recognized in the middle crust, and it is host to low-strain fabrics that record early stages of transpression in the Median Batholith.

Subsequent Separation Point Suite plutonism in Fiordland (including the Western Fiordland Orthogneiss in the lower crust) occurred over a broad, >70-km-wide, arc-perpendicular zone (Figs. 14B–14E). This zone of magmatism is significantly wider than the currently exposed width of the Jurassic to Early Cretaceous Darran Suite magmatic belt (Figs. 14A–14C). Whereas most active arcs are ~30–40 km wide and migrate laterally at 2–6 km m.y.$^{-1}$ (Ducea et al., 2015, 2017), this flare-up phase signaled both a widening and a geologically instantaneous continentward migration of arc magmatism at ca. 125 Ma (see Figs. 14C–14E). This voluminous surge of magmatism at all levels within the crust occurred during a period of regional thrusting, transpression, and crustal thickening throughout Fiordland (Daczko et al., 2001, 2002b; Klepeis et al., 2004; Marcotte et al., 2005; Allibone and Tulloch, 2008; Scott et al., 2011). This observation implies deformation was synchronous in middle and lower crust. In central Fiordland, this magmatic surge and widening of the arc coincided with the development of high-strain, mylonitic shear zones from ca. 125 to 116 Ma, and lower-crustal shearing continued to ca. 110–106 Ma.

Transpression and Melt Mobilization in Arc Crust

Our zircon and titanite geochronology indicate that transpressional shear zone development coincided spatially and temporally with the Early Cretaceous flare-up of Separation Point Suite plutons in the middle crust and lower crust. In the middle crust, Separation Point Suite plutons were largely focused into a broad, ~20-km-wide zone of regional transpression located in the western Lake Manapouri and southern Lake Te Anau area from ca. 129 to 110 Ma. In this region (the Grebe shear zone), large plutons such as the Puteketeke Pluton and West Arm Leucogranite display elongate map patterns with long axes that parallel the arc, the overall strike of low- and high-strain shear zones, and trends of S_2 mineral stretching lineations (Figs. 14B–14C). In the case of the Puteketeke Pluton, hypersolidus folding records shortening, and subvertical lineations in host rocks show evidence for vertical extrusion of midcrustal material during magma emplacement (Hufford, 2018; McGinn, 2018). The hypersolidus foliations and shortening in Puteketeke Pluton suggest that it was emplaced syntectonically during transpressional deformation within the ~20-km-wide Grebe shear zone. The high-Sr/Y character of the pluton further suggests that it originated from a lower-crustal magma reservoir, and these melts were mobilized and vertically transferred ~15 km or more to

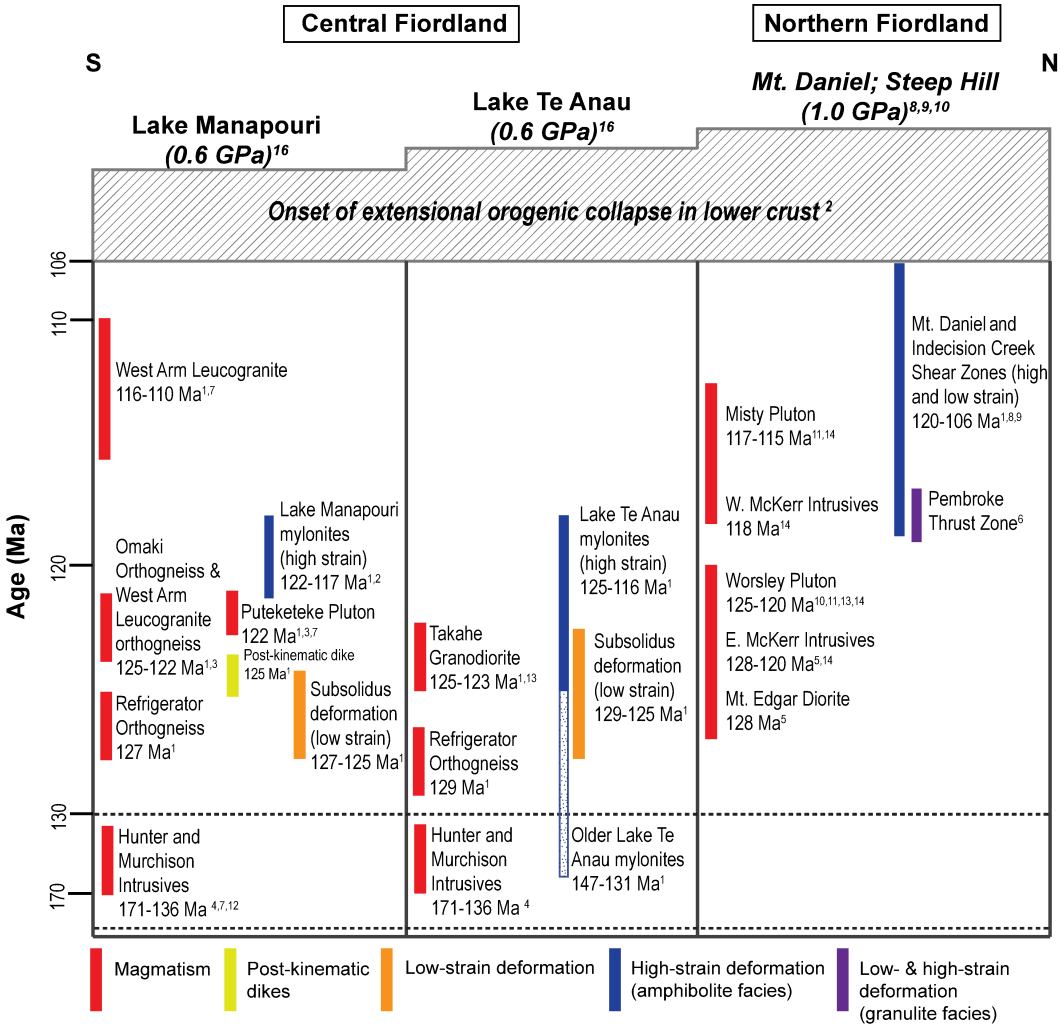

Figure 13. Time vs. space (S-N) diagram summarizing magmatic and metamorphic events in central and northern Fiordland. References: 1—this study, 2—Scott et al. (2009), 3—Ramezani and Tulloch (2009), 4—M. Ringwood, 2018, personal commun., 5—Hollis et al. (2003), 6—Daczko et al. (2002a), 7—Scott and Palin (2008), 8—Klepeis et al. (2004), 9—Marcotte et al. (2005), 10—Bhattacharya et al. (2018), 11—Milan et al. (2016), 12—Kimbrough et al. (1994), 13—Bolhar et al. (2008), 14—Schwartz et al. (2017).

midcrustal levels. Large mafic plutons in western Fiordland crystallized at this time and provide direct evidence for crystal accumulation in coeval lower-crustal storage regions (Allibone et al., 2009b; Milan et al., 2017; Schwartz et al., 2017).

In the lower crust of northern Fiordland, Marcotte et al. (2005) described evidence for synkinematic emplacement of dikes parallel and across mylonitic shear zones in the Indecision Creek shear zone. They reported that transpression in the lower crust involved vertical and non-vertical transport of material, including small volumes of melt within mylonitic shear zones. Work in the Pembroke granulite shows evidence for extensive melt migration through the lower crust at this time and that melt-rock interaction involved little crystallization of melt within the modified rocks (Stuart et al., 2016, 2017, 2018). That work, together with our new titanite ages, demonstrates that high-strain and subsolidus deformation outlasted emplacement of the Western Fiordland Orthogneiss by 10–15 m.y. (Figs. 13D–13E). Sustained high-temperature conditions (>650 °C) in the lower crust long after pluton emplacement (Gebauer, 2016) may have facilitated both high-temperature transpressional flow and extensional orogenic collapse in the lower crust (Klepeis et al., 2016; Schwartz et al., 2016).

CONCLUSIONS

Our U-Pb zircon geochronology data document the timing of Separation Point Suite magmatism in the middle crust of the Median Batholith (central Fiordland) from 129 to 110 Ma. Low-strain, subsolidus deformation (S_1, L_1) in the Refrigerator Orthogneiss occurred during the initiation of the Separation Point Suite flare-up event between ca. 129 and 125 Ma; however, subsolidus deformation is absent in the younger Separation Point Suite plutons that we observed. Titanite thermochronology reveals an important transition in the middle crust at ca. 125 Ma and continuing to ca. 116 Ma. This transition involved localized, amphibolite-facies mylonitic (S_2, L_2) deformation in the Lake Manapouri and Lake Te Anau mylonites. We found that transpressional deformation in Lake Manapouri is hosted

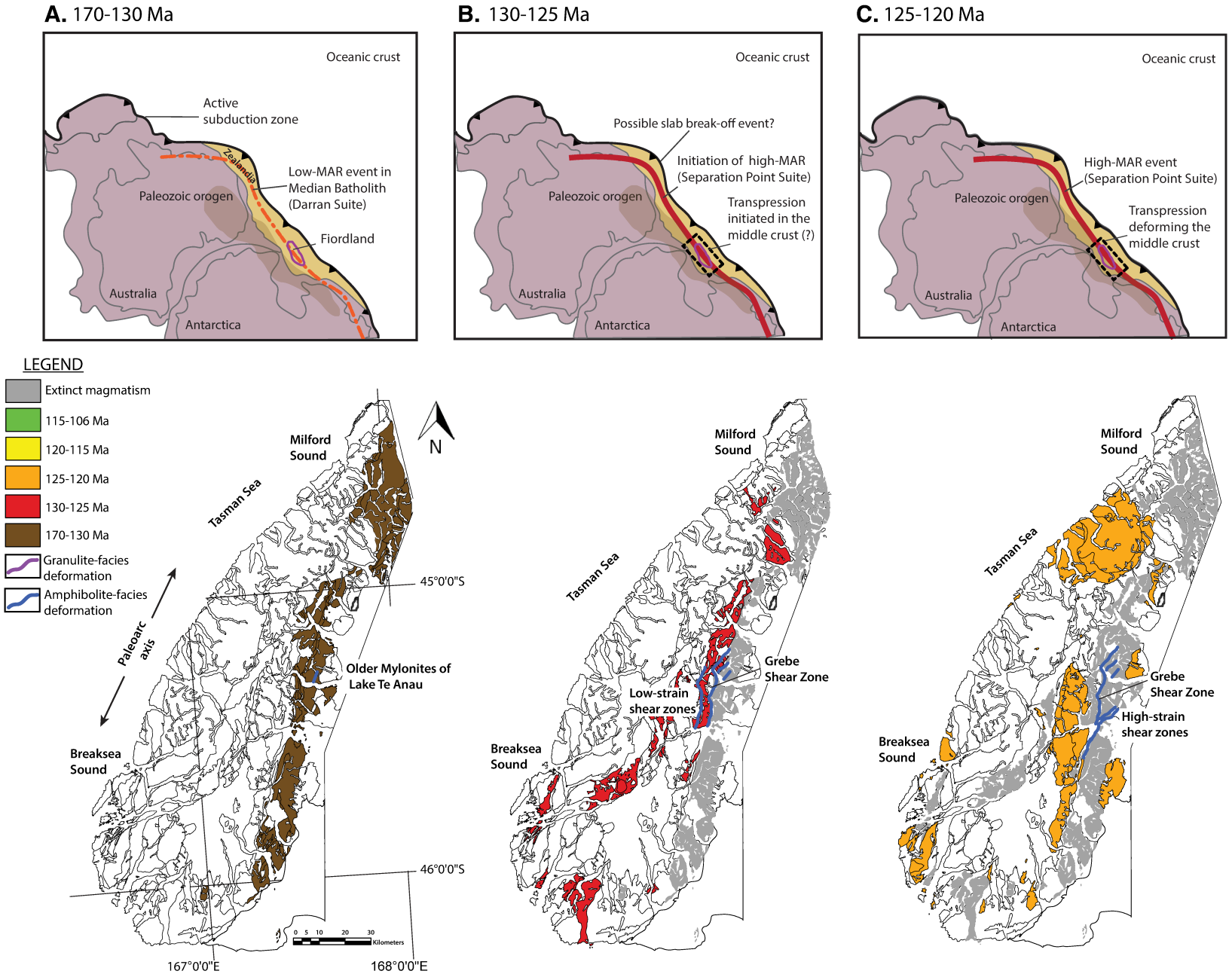

Figure 14. Time-magmatism-deformation maps of Fiordland from ca. 170 Ma to ca. 85 Ma. Maps were generated using $^{206}Pb/^{238}U$ zircon ages, and titanite chronology and thermometry data from this study and previous geochronologic and structural studies. Maps show the evolution of the Median Batholith magmatic arc, and widespread granulite- to amphibolite-facies metamorphism affecting both middle and lower crust. Zealandia palinspastic reconstructions show a Mesozoic orogenic convergent margin active until ca. 108 Ma, when extensional orogenic collapse initiated, leading to seafloor spreading and final split of Gondwana (Mortimer et al., 2017). (A) Darran Suite active from ca. 240 to 130 Ma. (*Continued on following page.*)

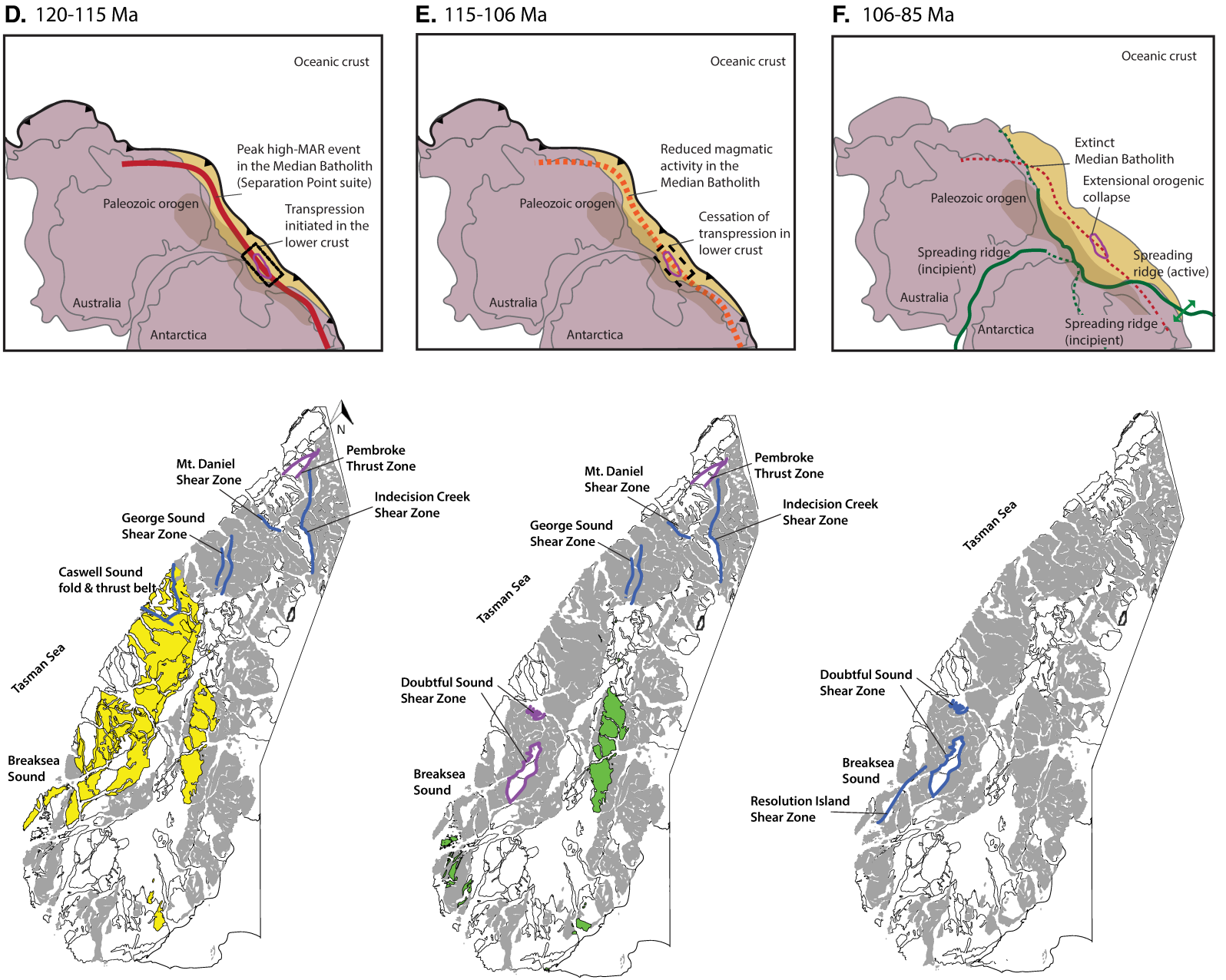

Figure 14 (*continued*). (B) Separation Suite magmatism initiated at ca. 129 Ma, coeval with low- to moderate-strain deformation in the middle crust. (C) Flare-up in Separation Suite took place ca. 125 Ma, and granulite- to amphibolite-facies deformation in the lower crust initiated by ca. 120 Ma. (D) Transpression in the lower and middle crust (granulite and amphibolite facies) was active and coeval ca. 120–115 Ma, and flare-up in Separation Point Suite continued. (E) Waning of Separation Point magmatism and end of transpression in the lower crust occurred between ca. 115 and 108 Ma. (F) Extensional orogenic collapse occurred after ca. 108–106 Ma. Fiordland maps are modified after Turnbull et al. (2010); Zealandia maps are modified after Mortimer and Campbell (2014). MAR—magma addition rate.

in Carboniferous rocks and is dated at ca. 122–117 Ma. Transpressional deformation during the ca. 125–116 Ma interval was synchronous in all branches of the Grebe shear zone, including a number of diffuse shear zones located in South Fiord, Lake Te Anau. In the lower crust (northern Fiordland), early transpressional fabrics are recorded by titanites in the Indecision Creek shear zone at ca. 118 Ma, and deformation at upper-amphibolite facies lasted in the Mount Daniel shear zone until ca. 110–106 Ma. A compilation of geochronological and structural data from the middle and lower crust suggests that magmatism generally preceded transpressional deformation within the arc, and that high-strain mylonitic deformation was associated with a voluminous surge of magmatism and the widening of the arc axis to 70 km or more during the peak flare-up stage (ca. 120–115 Ma). Highly elongate Separation Point Suite plutons in central Fiordland, and syndeformational features in the Puteketeke Pluton suggest that melts were focused into a broad, 20-km-wide zone of transpressional deformation in the middle crust. Similar, but lower-volume melt focusing was observed in lower crust (Indecision Creek shear zone; Marcotte et al., 2005), indicating that transpressional deformation was an important process in transporting lower-crustal melts to shallower levels and in controlling the distribution and the geometry of melt storage regions at midcrustal levels.

ACKNOWLEDGMENTS

We thank Peter Kuiper of Cruise Te Anau for assistance with rock sampling on Lake Te Anau and Lake Manapouri. Phoebe Shaw and the New Zealand Department of Conservation, Te Anau office, are also thanked for allowing access and sampling in Fiordland. Reviews by two anonymous reviewers significantly improved our manuscript. We also thank Richard Jongens and James Scott for insightful discussions. We thank Brad Ito for keeping the sensitive high-resolution mass spectrometer–reverse geometry (SHRIMP-RG) working so well and efficiently. Financial support for this work was provided by a California State University–Northridge Hannah Summer Fellowship (Buriticá), and National Science Foundation grants EAR-1352021 (Schwartz), EAR-1119248 (Klepeis), and EAR-1650219 (Miranda).

REFERENCES CITED

Allibone, A.H., and Tulloch, A.J., 2008, Early Cretaceous dextral transpressional deformation within the Median Batholith, Stewart Island, New Zealand: New Zealand Journal of Geology and Geophysics, v. 51, p. 115–134, https://doi.org/10.1080/00288300809509854.

Allibone, A.H., Turnbull, I.M., Tulloch, A.J., and Cooper, A.F., 2009a, Plutonic rocks of the Median Batholith in eastern and central Fiordland, New Zealand: Field relations, geochemistry, correlation, and nomenclature: New Zealand Journal of Geology and Geophysics, v. 52, p. 101–148, https://doi.org/10.1080/00288300909509882.

Allibone, A.H., Jongens, R., Turnbull, I.M., Milan, L.A., Daczko, N.R., De Paoli, M., and Tulloch, A.J., 2009b, Plutonic rocks of western Fiordland, New Zealand: Field relations, geochemistry, correlation, and nomenclature: New Zealand Journal of Geology and Geophysics, v. 52, p. 379–415, https://doi.org/10.1080/00288306.2009.9518465.

Bhattacharya, S., Kemp, A.I.S., and Collins, W.J., 2018, Response of zircon to melting and metamorphism in deep arc crust, Fiordland (New Zealand): Implications for zircon inheritance in cordilleran granites: Contributions to Mineralogy and Petrology, v. 173, no. 4, p. 28, https://doi.org/10.1007/s00410-018-1446-5.

Bitencourt, M. de F., and Nardi, L.V.S., 2000, Tectonic setting and sources of magmatism related to the southern Brazilian shear belt: Revista Brasileira de Geociencias, v. 30, p. 184–187, https://doi.org/10.25249/0375-7536.2000301186189.

Blanquat, M.D.S., Tikoff, B., Teyssier, C., and Vigneresse, J.L., 1998, Transpressional kinematics and magmatic arcs, *in* Holdsworth, R.E., Strachan, R.A., and Dewey, J.F., eds., Continental Transpressional and Transtensional Tectonics: Geological Society [London] Special Publication 135, p. 327–340, https://doi.org/10.1144/GSL.SP.1998.135.01.21.

Bolhar, R., Weaver, S.D., Palin, J.M., Cole, J.W., and Paterson, L.A., 2008, Systematics of zircon crystallisation in the Cretaceous Separation Point Suite, New Zealand, using U/Pb isotopes, REE and Ti geothermometry: Contributions to Mineralogy and Petrology, v. 156, p. 133–160, https://doi.org/10.1007/s00410-007-0278-5.

Brown, M., and Solar, G.S., 1998, Granite ascent and emplacement during contractional deformation in convergent orogens: Journal of Structural Geology, v. 20, p. 1365–1393, https://doi.org/10.1016/S0191-8141(98)00074-1.

Cao, M.J., Qin, K.Z., Li, G.M., Evans, N.J., and Jin, L.Y., 2015, In situ LA-(MC)-ICP-MS trace element and Nd isotopic compositions and genesis of polygenetic titanite from the Baogutu reduced porphyry Cu deposit, Western Junggar, NW China: Ore Geology Reviews, v. 65, p. 940–954, https://doi.org/10.1016/j.oregeorev.2014.07.014.

Cawood, P.A., Hawkesworth, C.J., and Dhuime, B., 2013, The continental record and the generation of continental crust: Geological Society of America Bulletin, v. 125, p. 14–32, https://doi.org/10.1130/B30722.1.

Chavez, T., Grace, R., and Stowell, H.H., 2007, New garnet Sm-Nd evidence for Paleozoic metamorphism, Wet Jacket Arm Fiordland, New Zealand: Geological Society of America Abstracts with Programs, v. 39, no. 4, p. 145–155.

Che, X.D., Linen, R.L., Wang, R.C., Groat, L.A., and Br, A.A., 2013, Distribution of trace and rare earth elements in titanite from tungsten and molybdenum deposits in Yukon and British Columbia, Canada: Canadian Mineralogist, v. 51, p. 415–438, https://doi.org/10.3749/canmin.51.3.415.

Cherniak, D.J., and Watson, E.B., 2000, Pb diffusion in rutile: Contributions to Mineralogy and Petrology, v. 172, p. 5–24, https://doi.org/10.1016/S0009-2541(00)00233-3.

Coble, M.A., Vazquez, J., Barth, A.P., Wooden, J., Burns, D., Kylander-Clark, A., Jackson, S., and Vennari, C.E., 2018, Trace element characterization of MAD-559 zircon reference material for ion microprobe analysis: Geostandards and Geoanalytical Research, v. 42, p. 481–497, https://doi.org/10.1111/ggr.12238.

Czertowicz, T.A., Scott, J.M., Waight, T.E., Palin, J.M., Van der Meer, Q.H.A., Le Roux, P., Munker, C., and Piazolo, S., 2016, The Anita Peridotite, New Zealand: Ultra-depletion and subtle enrichment in sub-arc mantle: Journal of Petrology, v. 57, p. 717–750, https://doi.org/10.1093/petrology/egw001.

Daczko, N.R., Klepeis, K.A., and Clarke, G.L., 2001, Evidence of Early Cretaceous collisional-style orogenesis in northern Fiordland, New Zealand, and its effects on the evolution of the lower crust: Journal of Structural Geology, v. 23, p. 693–713, https://doi.org/10.1016/S0191-8141(00)00130-9.

Daczko, N.R., Clarke, G.L., and Klepeis, K.A., 2002a, Kyanite-paragonite–bearing assemblages, northern Fiordland, New Zealand: Rapid cooling of the lower crustal root to a Cretaceous magmatic arc: Journal of Metamorphic Geology, v. 20, p. 887–902, https://doi.org/10.1046/j.1525-1314.2002.00421.x.

Daczko, N.R., Klepeis, K.A., and Clarke, G.L., 2002b, Thermomechanical evolution of the crust during convergence and deep crustal pluton emplacement in the western province of Fiordland, New Zealand: Tectonics, v. 21, p. 4-1–4-18, https://doi.org/10.1029/2001TC001282.

Daczko, N.R., Milan, L.A., and Halpin, J.A., 2009, Metastable persistence of pelitic metamorphic assemblages at the root of a Cretaceous magmatic arc—Fiordland, New Zealand: Journal of Metamorphic Geology, v. 27, p. 233–247, https://doi.org/10.1111/j.1525-1314.2009.00815.x.

Decker, M., Schwartz, J.J., Stowell, H.H., Klepeis, K.A., Tulloch, A.J., Kitajima, K., Valley, J.W., and Kylander-Clark, A.R.C., 2017, Slab-triggered arc flare-up in the Cretaceous Median Batholith and the growth of lower arc crust, Fiordland, New Zealand: Journal of Petrology, v. 58, p. 1145–1171, https://doi.org/10.1093/petrology/egx049.

Della Ventura, G., Bellatreccia, F., and Williams, C.T., 1999, Zr- and LREE-rich titanite from Tre Croci, Vico Volcanic complex (Latium, Italy): Mineralogical Magazine, v. 63, p. 123–130, https://doi.org/10.1180/002646199548240.

De Paoli, M.C., Clarke, G.L., Klepeis, K.A., Allibone, A.H., and Turnbull, I.M., 2009, The eclogite-granulite transition: Mafic and intermediate assemblages at Breaksea Sound, New Zealand: Journal of Petrology, v. 50, p. 2307–2343, https://doi.org/10.1093/petrology/egp078.

Dewey, J.F., Holdsworth, R.E., and Strachan, R.A., 1998, Transpression and transtension zones, *in* Holdsworth, R.E., Strachan, R.A., and Dewey, J.F., eds., Continental Transpressional and Transtensional Tectonics: Geological Society [London] Special Publication 135, p. 1–14, https://doi.org/10.1144/GSL.SP.1998.135.01.01.

Ducea, M.N., Saleeby, J.B., and Bergantz, G., 2015, The architecture, chemistry, and evolution of continental magmatic arcs: Annual Review of Earth and Planetary Sciences, v. 43, p. 299–331, https://doi.org/10.1146/annurev-earth-060614-105049.

Ducea, M.N., Bergantz, G., Crowley, J.L., and Otamendi, J., 2017, Ultrafast magmatic buildup and diversification to produce continental crust during subduction: Geology, v. 45, no. 3, p. 235–238, https://doi.org/10.1130/G38726.1.

Dwight, T., Scott, J.M., and Schwartz, J.J., 2018, Emplacement and Paleozoic and Cretaceous recrystallisation of the Broughton Arm Peridotite in western Fiordland, New Zealand: New Zealand Journal of Geology and Geophysics, v. 62, p. 72–86, https://doi.org/10.1080/00288306.2018.1528989.

Essex, R.M., and Gromet, L.P., 2000, U-Pb dating of prograde and retrograde titanite growth during the Scandian orogeny: Geology, v. 28, p. 419–422, https://doi.org/10.1130/0091-7613(2000)28<419:UDOPAR>2.0.CO;2.

Flowers, R.M., Bowring, S., Tulloch, A.J., and Klepeis, K.A., 2005, Tempo of burial and exhumation within the deep roots of a magmatic arc, Fiordland, New Zealand: Geology, v. 33, p. 17–20, https://doi.org/10.1130/G21010.1.

Fossen, H., and Cavalcante, G.C.G., 2017, Shear zones—A review: Earth-Science Reviews, v. 171, p. 434–455, https://doi.org/10.1016/j.earscirev.2017.05.002.

Fossen, H., Tikoff, B., and Teyssier, C., 1994, Strain modeling of transpressional and transtensional deformation: Norsk Geologisk Tidsskrift, v. 74, p. 134–145.

Franz, G., and Spear, F.S., 1985, Aluminous titanite (sphene) from the eclogite zone, south-central Tauern Window, Austria: Chemical Geology, v. 50, p. 33–46, https://doi.org/10.1016/0009-2541(85)90110-X.

Frost, B.R., Chamberlain, K.R., and Schumacher, J.C., 2001, Sphene (titanite): Phase relations and role as a geochronometer: Chemical Geology, v. 172, p. 131–148, https://doi.org/10.1016/S0009-2541(00)00240-0.

Fu, Y., Sun, X., Zhou, H., Lin, H., and Yang, T., 2016, In-situ LA-ICP-MS U-Pb geochronology and trace elements analysis of polygenetic titanite from the giant Beiya gold-polymetallic deposit in Yunnan Province, Southwest China: Ore Geology Reviews, v. 77, p. 43–56, https://doi.org/10.1016/j.oregeorev.2016.02.001.

Gao, X.Y., Zheng, Y.F., Chen, Y.X., and Guo, J., 2012, Geochemical and U-Pb age constraints on the occurrence of polygenetic titanites in UHP metagranite in the Dabie orogen: Lithos, v. 136–139, p. 93–108, https://doi.org/10.1016/j.lithos.2011.03.020.

Garber, J.M., Hacker, B., Kylander-Clark, A.R.C., Stearns, M., and Seward, G., 2017, Controls on trace element uptake in metamorphic titanite: Implications for petrochronology: Journal of Petrology, v. 58, p. 1031–1057, https://doi.org/10.1093/petrology/egx046.

Gebauer, S.K., 2016, Spatio-Temporal Patterns of Lower Arc Cooling and Metamorphism, Northern Fiordland, New Zealand [M.S. thesis]: Northridge, California, California State University–Northridge, 87 p.

Gollan, M., Palin, J.M., Faure, K., and Harris, C., 2005, Early Cretaceous upper crustal magmatism in southwest Fiordland: Geochronological and geochemical highlights, *in* Pettinga, J.R., and Wandres, A., eds., Geological Society of New Zealand 50th Annual Conference Program and Abstracts, Kaikoura, 2005: Geological Society of New Zealand Miscellaneous Publication 119A.

Harland, W.B., 1971, Tectonic transpression in Caledonian Spitsbergen: Geological Magazine, v. 108, p. 27–42, https://doi.org/10.1017/S0016756800050937.

Hayden, L.A., Watson, E.B., and Wark, D.A., 2008, A thermobarometer for sphene (titanite): Contributions to Mineralogy and Petrology, v. 155, p. 529–540, https://doi.org/10.1007/s00410-007-0256-y.

Hollis, J.A., Clarke, G.L., Klepeis, K.A., Daczko, N.R., and Ireland, T.R., 2003, Geochronology and geochemistry of high-pressure granulites of the Arthur River Complex, Fiordland, New Zealand: Cretaceous magmatism and metamorphism on the palaeo–Pacific margin: Journal of Metamorphic Geology, v. 21, p. 299–313, https://doi.org/10.1046/j.1525-1314.2003.00443.x.

Hufford, L.J., 2018, Strain Localization within Arc Crust: Microstructural Investigation of the Grebe Mylonite Zone in Fiordland, New Zealand [M.S. thesis]: Northridge, California, California State University–Northridge, 53 p.

Ireland, T.R., and Gibson, G.M., 1998, SHRIMP monazite and zircon geochronology of high-grade metamorphism in New Zealand: Journal of Metamorphic Geology, v. 16, p. 149–167, https://doi.org/10.1111/j.1525-1314.1998.00112.x.

Jagoutz, O., and Kelemen, P.B., 2015, Role of arc processes in the formation of continental crust: Annual Review of Earth and Planetary Sciences, v. 43, p. 363–404, https://doi.org/10.1146/annurev-earth-040809-152345.

Johnson, S.E., 2009, Magma extraction from the mantle wedge at convergent margins through dikes: A parametric sensitivity analysis: Geochemistry Geophysics Geosystems, v. 10, Q08017, https://doi.org/10.1029/2009GC002419.

Jones, R.R., Holdsworth, R.E., Clegg, P., McCaffrey, K., and Tavarnelli, E., 2004, Inclined transpression: Journal of Structural Geology, v. 26, p. 1531–1548, https://doi.org/10.1016/j.jsg.2004.01.004.

Kelemen, P.B., Hanghøj, K., and Greene, A.R., 2013, One view of the geochemistry of subduction-related magmatic arcs, with an emphasis on primitive andesite and lower crust, *in* Holland, H.D., and Turekian, K.K., eds., Treatise on Geochemistry (2nd ed.), Volume 4: Elsevier, p. 749–806, https://doi.org/10.1016/B978-0-08-095975-7.00323-5.

Kimbrough, D.L., Tulloch, A.J., Coombs, D.S., Landis, C.A., Johnston, M.R., and Mattinson, J.M., 1994, Uranium lead zircon ages from the Median Tectonic Zone, New Zealand: New Zealand Journal of Geology and Geophysics, v. 37, p. 393–419, https://doi.org/10.1080/00288306.1994.9514630.

Kirkland, C.L., Spaggiari, C.V., Johnson, T.E., Smithies, R.H., Danišík, M., Evans, N., Wingate, M.T.D., Clark, C., Spencer, C., Mikucki, E., and Mcdonald, B.J., 2016, Grain size matters: Implications for element and isotopic mobility in titanite: Precambrian Research, v. 278, p. 283–302, https://doi.org/10.1016/j.precamres.2016.03.002.

Klepeis, K.A., and Clarke, G.L., 2004, The evolution of an exposed mid-lower crustal attachment zone in Fiordland, New Zealand, *in* Grocott, J., McCaffrey, K.J.W., Taylor, G., and Tikoff, B., eds., Vertical Coupling and Decoupling in the Lithosphere: Geological Society [London] Special Publication 227, p. 197–229, https://doi.org/10.1144/GSL.SP.2004.227.01.11.

Klepeis, K.A., and King, D.S., 2009, Evolution of the middle and lower crust during the transition from contraction to extension in Fiordland, New Zealand: Geological Society of America Bulletin, v. 456, p. 243–265, https://doi.org/10.1130/2009.2456(09).

Klepeis, K.A., Daczko, N.R., Clarke, G L., 1999, Kinematic vorticity and tectonic significance of superposed mylonites in a major lower crustal shear zone, northern Fiordland, New Zealand: Journal of Structural Geology, v. 21, p. 1385–1405.

Klepeis, K.A., Clarke, G.L., and Rushmer, T., 2003, Magma transport and coupling between deformation and magmatism in the continental lithosphere: GSA Today, v. 13, no. 1, p. 4–11, https://doi.org/10.1130/1052-5173(2003)013<0004:MTACBD>2.0.CO;2.

Klepeis, K.A., Clarke, G.L., Gehrels, G., and Vervoort, J., 2004, Processes controlling vertical coupling and decoupling between the upper and lower crust of orogens: Results from Fiordland, New Zealand: Journal of Structural Geology, v. 26, p. 765–791, https://doi.org/10.1016/j.jsg.2003.08.012.

Klepeis, K.A., King, D., De Paoli, M., Clarke, G.L., and Gehrels, G., 2007, Interaction of strong lower and weak middle crust during lithospheric extension in western New Zealand: Tectonics, v. 26, TC4017, https://doi.org/10.1029/2006TC002003.

Klepeis, K.A., Schwartz, J., Stowell, H., and Tulloch, A., 2016, Gneiss domes, vertical and horizontal mass transfer, and the initiation of extension in the hot lower-crustal root of a continental arc, Fiordland, New Zealand: Lithosphere, v. 8, p. 116–140, https://doi.org/10.1130/L490.1.

Klepeis, K.A., Webb, L., Blatchford, H., Schwartz, J.J., Jongens, R., Turnbull, R., and Stowell, H.H., 2019, Deep slab collision during Miocene subduction causes uplift along crustal-scale reverse faults in Fiordland, New Zealand: GSA Today, v. 29, https://doi.org/10.1130/GSATG399A.1.

Kohn, M.J., and Corrie, S.L., 2011, Preserved Zr-temperatures and U-Pb ages in high-grade metamorphic titanite: Evidence for a static hot channel in the Himalayan orogen: Earth and Planetary Science Letters, v. 311, p. 136–143, https://doi.org/10.1016/j.epsl.2011.09.008.

Kylander-Clark, A.R.C., Hacker, B.R., and Cottle, J.M., 2013, Laser-ablation split-stream ICP petrochronology: Chemical Geology, v. 345, p. 99–112, https://doi.org/10.1016/j.chemgeo.2013.02.019.

Little, T.A., Cox, S., Vry, J.K., and Batt, G., 2005, Variations in exhumation level and uplift rate along the oblique-slip Alpine fault, central Southern Alps, New Zealand: Geological Society of America Bulletin, v. 117, p. 707–723, https://doi.org/10.1130/B25500.1.

Loader, M.A., Wilkinson, J.J., and Armstrong, R.N., 2017, The effect of titanite crystallisation on Eu and Ce anomalies in zircon and its implications for the assessment of porphyry Cu deposit fertility: Earth and Planetary Science Letters, v. 472, p. 107–119, https://doi.org/10.1016/j.epsl.2017.05.010.

Marcotte, S.B., Klepeis, K.A., Clarke, G.L., Gehrels, G., and Hollis, J.A., 2005, Intra-arc transpression in the lower crust and its relationship to magmatism in a Mesozoic magmatic arc: Tectonophysics, v. 407, p. 135–163, https://doi.org/10.1016/j.tecto.2005.07.007.

Matzel, J.E.P., Bowring, S.A., and Miller, R.B., 2006, Time scales of pluton construction at differing crustal levels: Examples from the Mount Stuart and Tenpeak intrusions, North Cascades, Washington: Geological Society of America Bulletin, v. 118, p. 1412–1430, https://doi.org/10.1130/B25923.1.

McGinn, C., 2018, Effects of Quartz Dauphiné Twinning on Strain Localization in Polymineralic Rocks in a Mid-Crustal Shear Zone, Fiordland, New Zealand: Northridge, California, California State University–Northridge, 51 p.

Meert, J.G., 2003, Proterozoic East Gondwana: Supercontinent Assembly and Breakup, Special Publication 206: Eos (Transactions, American Geophysical Union), v. 84, no. 37, p. 372–372, https://doi.org/10.1029/2003EO370012.

Milan, L.A., Daczko, N.R., Clarke, G.L., and Allibone, A.H., 2016, Complexity of in-situ zircon U-Pb-Hf isotope systematics during arc magma genesis at the roots of a Cretaceous arc, Fiordland, New Zealand: Lithos, v. 264, p. 296–314, https://doi.org/10.1016/j.lithos.2016.08.023.

Milan, L.A., Daczko, N.R., and Clarke, G.L., 2017, Cordillera Zealandia: A Mesozoic arc flare-up on the palaeo-Pacific Gondwana margin: Scientific Reports, v. 7, p. 261, https://doi.org/10.1038/s41598-017-00347-w.

Mortimer, N., 2004, New Zealand's geological foundations: Gondwana Research, v. 7, p. 261–272, https://doi.org/10.1016/S1342-937X(05)70324-5.

Mortimer, N., and Campbell, H., 2014, Zealandia: Our Continent Revealed: Rosedale, Auckland, New Zealand, Penguin Random House New Zealand, 272 p.

Mortimer, N., Gans, P., Calvert, A., and Walker, N., 1999a, Geology and thermochronometry of the east edge of the Median Batholith (Median Tectonic Zone): A new perspective on Permian to Cretaceous crustal growth of New Zealand: The Island Arc, v. 8, p. 404–425, https://doi.org/10.1046/j.1440-1738.1999.00249.x.

Mortimer, N., Tulloch, A.J., Spark, R.N., Walker, N.W., Ladley, E., Allibone, A., and Kimbrough, D.L., 1999b, Overview of the Median Batholith, New Zealand: A new interpretation of the geology of the Median Tectonic Zone and adjacent rocks: Journal of African Earth Sciences, v. 29, p. 257–268, https://doi.org/10.1016/S0899-5362(99)00095-0.

Mortimer, N., Campbell, H.J., Tulloch, A.J., King, P.R., Stagpoole, V.M., Wood, R.A., Rattenbury, M.S., Sutherland, R., Adams, C.J., Collot, J., and Seton, M., 2017, Zealandia: Earth's hidden continent: GSA Today, v. 27, no. 3, p. 27–35, https://doi.org/10.1130/GSATG321A.1.

Muir, R.J., Ireland, T.R., Weaver, S.D., Bradshaw, J.D., Evans, J.A., Eby, G.N., and Shelley, D., 1998, Geochronology and geochemistry of a Mesozoic magmatic arc system, Fiordland, New Zealand: Journal of the Geological Society [London], v. 155, p. 1037–1053, https://doi.org/10.1144/gsjgs.155.6.1037.

Olin, P.H., and Wolff, J.A., 2012, Partitioning of rare earth and high field strength elements between titanite and phonolitic liquid: Lithos, v. 128–131, p. 46–54, https://doi.org/10.1016/j.lithos.2011.10.007.

Paterson, S.R., and Schmidt, K.L., 1999, Is there a close spatial relationship between faults and plutons?: Journal of Structural Geology, v. 21, p. 1131–1142, https://doi.org/10.1016/S0191-8141(99)00024-3.

Paterson, S.R., Fowler, T.K., Jr., Schmidt, K.L., Yoshinobu, A.S., Yuan, E.S., and Miller, R.B., 1998, Interpreting magmatic fabric patterns in plutons: Lithos, v. 44, p. 53–82, https://doi.org/10.1016/S0024-4937(98)00022-X.

Pennacchioni, G., 2005, Control of the geometry of precursor brittle structures on the type of ductile shear zone in the Adamello tonalites, southern Alps (Italy): Journal of Structural Geology, v. 27, no. 4, p. 627–644, https://doi.org/10.1016/j.jsg.2004.11.008.

Pereira, M.F., Chichorro, M., Fernández, C., Silva, J.B., and Matias, F.V., 2013, The role of strain localization in magma injection into a transtensional shear zone (Variscan belt, SW Iberia): Journal of the Geological Society [London], v. 170, p. 93–105, https://doi.org/10.1144/jgs2012-008.

Ramsay, J.G., and Huber, M.I., 1983, The techniques of modern structural geology: Strain analysis, Volume 1: Academic press, 307 p.

Ramezani, J., and Tulloch, A.J., 2009, TIMS U-Pb geochronology of southern and eastern Fiordland: GNS Science, https://doi.org/10.21420/G2CC7Z.

Sanderson, D.J., and Marchini, W.R.D., 1984, Transpression: Journal of Structural Geology, v. 6, p. 449–458, https://doi.org/10.1016/0191-8141(84)90058-0.

Schmidt, K.L., and Paterson, S.R., 2000, Analyses fail to find coupling between deformation and magmatism: Eos (Transactions, American Geophysical Union), v. 81, p. 197–203, https://doi.org/10.1029/00EO00133.

Schwartz, J.J., Stowell, H.H., Klepeis, K.A., Tulloch, A.J., Kylander-Clark, A.R.C.C., Hacker, B.R., and Coble, M.A., 2016, Thermochronology of extensional orogenic collapse in the deep crust of Zealandia: Geosphere, v. 12, p. 647–677, https://doi.org/10.1130/GES01232.1.

Schwartz, J.J., Klepeis, K.A., Sadorski, J.F., Stowell, H.H., Tulloch, A.J., and Coble, M.A., 2017, The tempo of continental arc construction in the Mesozoic Median Batholith, Fiordland, New Zealand: Lithosphere, v. 9, no. 3, p. 343–365, https://doi.org/10.1130/L610.1.

Scibiorski, E., Kirkland, C.L., Kemp, A.I.S., Tohver, E., and Evans, N.J., 2019, Trace elements in titanite: A potential tool to constrain polygenetic growth processes and timing: Chemical Geology, v. 509, p. 1–19, https://doi.org/10.1016/j.chemgeo.2019.01.006.

Scott, J., 2013, A review of the location and significance of the boundary between the Western Province and Eastern Province, New Zealand: New Zealand Journal of Geology and Geophysics, v. 56, p. 276–293, https://doi.org/10.1080/00288306.2013.812971.

Scott, J.M., and Palin, J.M., 2008, LA-ICP-MS U-Pb zircon ages from Mesozoic plutonic rocks in eastern Fiordland, New Zealand: New Zealand Journal of Geology and Geophysics, v. 51, p. 105–113, https://doi.org/10.1080/00288300809509853.

Scott, J.M., Cooper, A.F., Palin, J.M., Tulloch, A.J., Kula, J., Jongens, R., Spell, T.L., and Pearson, N.J., 2009, Tracking the influence of a continental margin on growth of a magmatic arc, Fiordland, New Zealand, using thermobarometry, thermochronology, and zircon U-Pb and Hf isotopes: Tectonics, v. 28, TC6007, https://doi.org/10.1029/2009TC002489.

Schwartz_L1073 2nd pages / 30 of 31

Scott, J.M., Cooper, A.F., Tulloch, A.J., and Spell, T.L., 2011, Crustal thickening of the Early Cretaceous paleo-Pacific Gondwana margin: Gondwana Research, v. 20, p. 380–394, https://doi.org/10.1016/j.gr.2010.10.008.

Sen, K., Mukherjee, B.K., and Collins, A.S., 2014, Interplay of deformation and magmatism in the Pangong transpression zone, eastern Ladakh, India: Implications for remobilization of the trans-Himalayan magmatic arc and initiation of the Karakoram fault: Journal of Structural Geology, v. 62, p. 13–24, https://doi.org/10.1016/j.jsg.2014.01.009.

Smith, M.P., Storey, C.D., Jeffries, T.E., and Ryan, C., 2009, In situ U-Pb and trace element analysis of accessory minerals in the Kiruna District, Norrbotten, Sweden: New constraints on the timing and origin of mineralization: Journal of Petrology, v. 50, p. 2063–2094, https://doi.org/10.1093/petrology/egp069.

Spencer, K.J., Hacker, B.R., Kylander-Clark, A.R.C., Andersen, T.B., Cottle, J.M., Stearns, M.A., Poletti, J.E., and Seward, G.G.E., 2013, Campaign-style titanite U-Pb dating by laser-ablation ICP: Implications for crustal flow, phase transformations and titanite closure: Chemical Geology, v. 341, p. 84–101, https://doi.org/10.1016/j.chemgeo.2012.11.012.

Stearns, M.A., Hacker, B.R., Ratschbacher, L., Rutte, D., and Kylander-Clark, A.R.C., 2015, Titanite petrochronology of the Pamir gneiss domes: Implications for middle to deep crust exhumation and titanite closure to Pb and Zr diffusion: Tectonics, v. 34, p. 784–802, https://doi.org/10.1002/2014TC003774.

Storey, C.D., Jeffries, T.E., and Smith, M., 2006, Common lead–corrected laser ablation ICP-MS U-Pb systematics and geochronology of titanite: Chemical Geology, v. 227, p. 37–52, https://doi.org/10.1016/j.chemgeo.2005.09.003.

Stowell, H., Tulloch, A., Zuluaga, C., and Koenig, A., 2010, Timing and duration of garnet granulite metamorphism in magmatic arc crust, Fiordland, New Zealand: Chemical Geology, v. 273, p. 91–110, https://doi.org/10.1016/j.chemgeo.2010.02.015.

Stuart, C.A., Piazolo, S., and Daczko, N.R., 2016, Mass transfer in the lower crust: Evidence for incipient melt assisted flow along grain boundaries in the deep arc granulites of Fiordland, New Zealand: Geochemistry Geophysics Geosystems, v. 17, p. 3733–3753, https://doi.org/10.1002/2015GC006236.

Stuart, C.A., Daczko, N.R., and Piazolo, S., 2017, Local partial melting of the lower crust triggered by hydration through melt-rock interaction: An example from Fiordland, New Zealand: Journal of Metamorphic Geology, v. 35, p. 213–230, https://doi.org/10.1111/jmg.12229.

Stuart, C.A., Piazolo, S., and Daczko, N.R., 2018, The recognition of former melt flux through high-strain zones: Journal of Metamorphic Geology, v. 36, p. 1049–1069, https://doi.org/10.1111/jmg.12427.

Tulloch, A.J., and Kimbrough, D., 2003, Paired plutonic belts in convergent margins and the development of high Sr/Y magmatism: Peninsular Ranges Batholith of Baja California and Median Batholith of New Zealand, *in* Johnson, S.E., Paterson, S.R., Fletcher, J.M., Girty, G.H., Kimbrough, D.L., and Martín-Barajas, A., eds., Tectonic Evolution of Northwestern México and the Southwestern USA: Geological Society of America Special Paper 374, p. 275–296, https://doi.org/10.1130/0-8137-2374-4.275.

Tulloch, A.J., Ramezani, J., Kimbrough, D.L., Faure, K., and Allibone, H., 2009, U-Pb geochronology of mid-Paleozoic plutonism in western New Zealand: Implications for S-type granite generation and growth of the east Gondwana margin: Geological Society of America Bulletin, v. 121, p. 1236–1261, https://doi.org/10.1130/B26272.1.

Tulloch, A.J., Ireland, T.R., Kimbrough, D.L., Griffin, W.L., and Ramezani, J., 2011, Autochthonous inheritance of zircon through Cretaceous partial melting of Carboniferous plutons: The Arthur River Complex, Fiordland, New Zealand: Contributions to Mineralogy and Petrology, v. 161, no. 3, p. 401–421, https://doi.org/10.1007/s00410-010-0539-6.

Turnbull, I.M., Allibone, A.H., and Jongens, R., compilers, 2010, Geology of the Fiordland Area: Lower Hutt, New Zealand, GNS Science, Institute of Geological & Nuclear Sciences Geological Map 17, 97 p. + 1 folded map (scale 1:250,000).

Turnbull, R.E., Tulloch, A.J., Ramezani, J., and Jongens, R., 2016, Extension-facilitated pulsed S-I-A–type "flare-up" magmatism at 370 Ma along the southeast Gondwana margin in New Zealand: Insights from U-Pb geochronology and geochemistry: Geological Society of America Bulletin, v. 128, p. 1500–1520, https://doi.org/10.1130/B31426.1.

Vermeesch, P., 2018, IsoplotR: A free and open toolbox for geochronology: Geoscience Frontiers, v. 9, p. 1479–1493, https://doi.org/10.1016/j.gsf.2018.04.001.

Vigneresse, J.L., 1995, Crustal regime of deformation and ascent of granitic magma: Tectonophysics, v. 249, p. 187–202, https://doi.org/10.1016/0040-1951(95)00005-8.

Vigneresse, J.L., and Clemens, J.D., 2000, Granitic magma ascent and emplacement: Neither diapirism nor neutral buoyancy, *in* Vendeville, B.C., Mart, Y., and Vigneresse, J.L., eds., Salt, Shale and Igneous Diapirs in and around Europe: Geological Society [London] Special Publication 174, p. 1–19, https://doi.org/10.1144/GSL.SP.1999.174.01.01.

Watson, E.B., Wark, D.A., and Thomas, J.B., 2006, Crystallization thermometers for zircon and rutile: Contributions to Mineralogy and Petrology, v. 151, https://doi.org/10.1007/s00410-006-0068-5.

Webber, J.R., Klepeis, K.A., Webb, L.E., Cembrano, J., Morata, D., Mora-Klepeis, G., and Arancibia, G., 2015, Deformation and magma transport in a crystallizing plutonic complex, Coastal Batholith, central Chile: Geosphere, v. 11, no. 5, p. 1401–1426, https://doi.org/10.1130/GES01107.1.

Weinberg, R.F., Sial, A.N., and Mariano, G., 2004, Close spatial relationship between plutons and shear zones: Geology, v. 32, p. 377–380, https://doi.org/10.1130/G20290.1.

Weinberg, R.F., Mark, G., and Reichardt, H., 2009, Magma ponding in the Karakoram shear zone, Ladakh, NW India: Geological Society of America Bulletin, v. 121, p. 278–285, https://doi.org/10.1130/B26358.1.

Whitney, D.L., and Evans, B.W., 2010, Abbreviations for names of rock-forming minerals: The American Mineralogist, v. 95, p. 185–187, https://doi.org/10.2138/am.2010.3371.

Whitney, D.L., Teyssier, C., and Rey, P.F., 2009, The consequences of crustal melting in continental subduction: Lithosphere, v. 1, p. 323–327, https://doi.org/10.1130/L62.1.

MANUSCRIPT RECEIVED 25 FEBRUARY 2019
REVISED MANUSCRIPT RECEIVED 19 MAY 2019
MANUSCRIPT ACCEPTED 28 JUNE 2019